Ph.D. DISSERTATION

Highly Improved Response and Recovery Characteristics of FET-type Gas Sensor using Pre-Bias

Pre-bias 펄스 측정을 이용한 FET-type 가스센서의 응답 및 복구 특성 향상

BY

JONGMIN SHIN

February 2018

DEPARTMENT OF ELECTRICAL ENGINEERING AND
COMPUTER SCIENCE
COLLEGE OF ENGINEERING
SEOUL NATIONAL UNIVERSITY

Highly Improved Response and Recovery Characteristics of FET-type Gas Sensor using Pre-Bias

Pre-bias 펄스 측정을 이용한 FET-type 가스센서의 응답 및 복구 특성 향상

지도교수 이 종 호

이 논문을 공학박사 학위논문으로 제출함

2018 년 2 월

서울대학교 대학원

전기컴퓨터공학부

신 종 민

신종민의 공학박사 학위논문을 인준함

2018 년 2 월

위 원 장 : 박 병 국 (인)

부위원장 : 이 종 호 (인)

위 원 : 황 철 성 (인)

위 원 : 장 호 원 (인)

위 원 : 권 혁 인 (인)

ABSTRACT

Recently, a gas sensor technology has become increasingly important due to the increasing demand for automobiles, air quality control, farming, and household appliances. Thus sensor technology is expected to play an important role in the Internet of Things (IoT) era. Various types of gas sensors such as optical, electrochemical, semiconducting and FET-based gas sensors have been widely reported so far. However, most of the studies on the gas sensors have been focused on resistor-type sensors and the investigation of sensing materials rather than the electrical control scheme. The resistor-type sensor has demerits in size, yield, and integration with CMOS circuits. Thus, to fulfill the demands for low cost, scalable, stable, and CMOS compatibility for the gas sensor, FET-type sensors have been widely studied. Although the FET-type sensors have a higher degree of freedom coming from four terminal features in enhancing the sensing performance, there have been no report on electrical control scheme.

In this dissertation, we propose, for the first time, a pulse pre-bias scheme for enhancing the sensing performance of Si FET-type gas sensor and investigate the pre-bias effect on the response and recovery characteristics. The Si FET type gas sensor having a control-gate (CG) and a floating-gate (FG) in horizontal direction is fabricated to investigate the pre-bias effect. The ZnO film as a

sensing material is deposited between the CG and the FG by ALD. By applying the pulse bias scheme to the CG of the FET-type gas sensor, the pre-bias effect is verified, and we analyze the reaction between NO_2 gas and the ZnO as a sensing layer deposited on the Si FET-type gas sensor. The mechanism responsible for the pre-bias effect is explained using energy band diagram.

The proposed scheme was verified to be very efficient in improving the gas response and the reduction of the recovery time to NO_2 target gas. It is expected that the pre-biasing scheme will be very practical in the commercialization of the FET-type gas sensor.

Keywords: pulse pre-bias scheme, FET-type gas sensor, low power, work-function change, capacitance change

Student number: 2012-20801

CONTENTS

Abstract.....i

Contents.....v

List of Figures.....ix

List of Tables.....xvi

Chapter 1

Introduction.....1

1.1 Study background.....1

1.1.1 Motivation…….....1

1.1.2 Improvement of gas sensing characteristics…….....7

1.2 Purpose of research.....11

1.3 Thesis outline.....12

Chapter 2

Device structures and fabrications.....13

2.1 Device structure.....13

2.2 Device fabrication.....17

2.2.1 Key fabrication process….....27

2.2.2 Simulation study for buried channel implantation.....22

2.2.3 Formation of sensing layer.....25

Chapter 3

Device characteristics..... 28

3.1 *I_V* characteristics of FET-type gas sensor.....28

3.2 Electrical modeling of FET-type gas sensor.....32

3.3 Nonvolatile functionality.....37

3.4 Gas sensing mechanisms of the FET-type gas sensor.....40

3.5 Resistor-type gas sensor.....44

Chapter 4

Proposed pulse per-bias scheme and gas sensing characteristics.....48

4.1 Motivation.....48

4.2 Proposed pulse pre-bias scheme.....50

4.3 The pre-bias effect.....52

4.3.1 The pre-bias effect on gas response.....52

4.3.2 Mechanism responsible for the gas response.....55

4.3.3 The pre-bias effect on gas recovery.....60

4.3.4 Mechanism responsible for the gas recovery.....62

4.4 Gas response to different concentration of NO_2 gas.....64

4.5 Optimal pulse pre-bias scheme for oxidizing gas.....70

4.6 The advantages of the pre-bias effect.....74

4.7 The pre-bias effect on reducing gas in recovery period.....76

Chapter 5

Conclusions.....78

Appendix A.

Considerations for the pulse pre-bias scheme.....80

A.1 Effect of the pulse with of pre-bias 80

A.2 Effect of the carrier gas 81

Appendix B.

Capacitance change FET-type gas sensor.....82

Bibliography.....84

List of Publications.....92

Abstract in Korean.....98

List of Figures

Figure 1.1. Semiconducting gas sensor currently being produced by FIGARO, Japan. 2

Figure 1.2. Si FET-type gas sensor having a suspended gate structure. There is an air gap between the control gate and the floating gate, and a sensing layer formed right below the CG [23]. 4

Figure 1.3. C.H. kim *et al.* reported the Si FET-type gas sensor having a floating gate [27]. 5

Figure 1.4. Various types of metal oxide hollow spheres for gas sensing material reported by Prof. J.H. Lee's research group. http://fnml.korea.ac.kr [38]. 6

Figure 1.5. Enhancement gas adsorption and desorption by UV illumination [41]. 9

Figure 1.6. The heating effect of the sensing material in oxygen ambience [41]. 9

Figure 1.7. Embedded micro-heater in the resistor-type gas sensor [42]. 10

Figure 2.1. (a) Top SEM image of the fabricated FET-type gas sensor. (b) Surface SEM views of the ZnO layer formed on SiO_2 (top) and FG (bottom). Schematic cross-sectional view of the fabricated FET-type gas sensor cut along the yellow dashed line A-

A’ (c) and the red dashed line B-B’(c).....14

Figure 2.2. Schematic cross-sectional views of key fabrication process steps of the FET-type sensor cut along a yellow dashed line A-A’ in Fig. 2.1 (a). By using five mask steps, the FET-type gas sensor can be fabricated including sensing layer.....15

Figure 2.3. (a) SEM images of the active region of the MOSFET after growing the field oxide and (b) define active region after etching Si_3N_4 and pad oxide.....17

Figure 2.4. Simulated I_D-V_G curves as a parameter of BF_2^+ ion dose.....22

Figure 2.5. Measured I_D-V_G curves of the fabricated MOSFET as a parameter of BF_2^+ ion.....22

Figure 2.6. XPS survey spectra of ZnO. The ZnO as a sensing layer is deposited by ALD. The formed ZnO film shows a peak of Zn2p3 (1022.08 eV) and O 1s (532.08 eV) which is consistent with the reported value of ZnO.....25

Figure 3.1. The pulse wave form used for the PIV.....26

Figure 3.2. (a) Transfer (I_D-V_{CG}) curves of the *p*MOSFET sensor measured by the DC and PIV methods as a parameter of T (20 ^oC, and 160-220 ^oC) at V_{DS} = -0.1 V. (b)

Output characteristics of the *p*MOSFET sensor measured by the DC and PIV methods at T = 180 °C. 28

Figure 3.3. (a) Schematic cross-sectional view of the FET-type gas sensor. In this research, the ZnO is used as a sensing material. (b) Magnified region of the black dashed line in (a). (c) Equivalent circuit model of the gas sensor along a red dashed line A-A' in Fig. 3.3 (a). (d) Simplified equivalent circuit of the gas sensor. 32

Figure 3.4. Program and erase characteristics of the FET-type gas sensor as parameters of the program voltage (V_{PGM}) and erase voltage (V_{ERS}). 34

Figure 3.5. Retention characteristics of the fabricated gas sensor. The V_{th} shifts are negligible up to 10^4 s. 35

Figure 3.6. (a) Top SEM image of the fabricated resistor-type gas sensor. (b) Schematic cross sectional view of the fabricated resistor-type gas sensor cut along a yellow dashed line A-A' in (a). 42

Figure 3.7. *I-V* curves of the resistor-type gas sensor at RT (20 °C) and 180 °C. 42

Figure 3.8. Transient *I* behaviors of the resistor-type gas sensor as a parameter of NO_2 concentrations (0.25 ppm, 0.5 ppm, 1.25 ppm, and 2.5 ppm) at 180 °C. 43

Figure 4.1 Temperature effect on FET-type gas sensor in ref [28]. 45

Figure 4.2. Schematic image of the measurement system. 47

Figure 4.3. Proposed pulse scheme for the pre-bias (V_{pre}) and read bias (V_{rCG}). The V_{pre} and V_{rCG} are applied to the CG alternatively with respective pulse widths of t_{pre} and t_{read}. 47

Figure 4.4. (a) Transient I_D behaviors with different V_{pre}s in 0.5 ppm of NO_2. (b) Gas response versus V_{pre}, which is calculated by the equation (8) using measured I_D at t = 70 s in Fig. 4.4 (a). 49

Figure 4.5. Energy band diagram of the *p*MOSFET sensor at flat band condition. 51

Figure 4.6. Energy band diagram of the *p*MOSFET sensor in (a) pre-bias period by applying negative V_{pre} and (b) read period (V_{rCG} = 0 V) in air ambience. 51

Figure 4.7. Schematic energy band diagrams of the gas sensor in the pre-bias period at different V_{pre}s and read period at a V_{rCG} of 0 V. The solid and the dashed lines stand for the energy band diagrams before and after NO_2 exposure, respectively. Adsorbed NO_2 molecules can be represented as a local acceptor. The area of the rectangle at the interface represents the total amount of possible sites for the adsorption of NO_2 molecules and the filled area schematically refers to the amount of extracted electrons.....52

Figure 4.8. (a) Transient I_D behaviors with different V_{pre}s (-1 V ~ 4 V) during the recovery period (t > 76 s). In the response period (10 < t < 73 s), the V_{pre} is fixed at -1 V. (b) Recovery versus V_{pre} as a parameter of sampling time in the recovery period. 57

Figure 4.9. (a) Response with a negative V_{pre} and recovery with a positive V_{pre}. (b) Schematic energy band diagram to explain desorption of NO_2 with a positive V_{pre} during recovery period. The sequence of the desorption is depicted by ① and ②. 59

Figure 4.10. Transient I_D behaviors as a parameter of gas concentration at V_{pre} = -2 V. 63

Figure 4.11. Gas response versus gas concentration as a parameter of V_{pre} (from -2 V to 2 V). The insert represents gas response versus V_{pre} at 0.25 ppm. 63

Figure 4.12. (a) Transient I_D behaviors and (b) response of the FET-type gas sensor as a function of NO_2 concentration on a logarithmic scale at -2 V of V_{pre}. The FET-type gas sensor can detect 25 ppb of NO_2. 64

Figure 4.13. (a) I_D-V_{CG} curves as a parameter of the NO_2 concentration at 180 °C. (b) V_{th} shift versus NO_2 concentration from 25 ppb to 500 ppb. 65

Figure 4.14. Optimal pulse pre-bias scheme for oxidizing gas. 68

Figure 4.15. Repeated 0.5 ppm NO_2 gas responses measured at 180 °C. The V_{pre}s for the response and recovery periods are -1 V and 2 V, respectively. V_{rCG} and V_{rDS} pulses are fixed at 0 V and -0.1 V, respectively. 69

Figure 4.16. Comparison of the recovery characteristics with DC measurement at different temperature from 160 °C to 220 °C by applying V_{CG} of 0 V. Responses represented by solid line and symbol are measured data with different V_{pre} from 1 V to 4 V in the recovery period at 180 °C. In the response period, V_{pre} of -1V is applied to the CG. 71

Figure 4.17. Transient I_D behaviors with different V_{pre}s in 16 ppm of H_2S at 180 °C. ...77

Figure A.1. Transient I_D behaviors as a parameter of t_{pre}s from 500 μs to 0.1s in response period. 80

Figure A.2. The effect of the carrier gas. 81

Figure B.1. (a) Mask layout of the CFET gas sensor. (b) Schematic cross-sectional view of the CFET gas sensor along the dotted line in (a). 83

Chapter 1

Introduction

1.1 Study background

1.1.1 Motivation

Recently, a gas sensor technology has become increasingly important due to the increasing demand for automobiles, air quality control, farming, and household appliances [1-4]. Thus sensor technology is expected to play an important role in the Internet of Things (IoT) era. Due to seriousness of indoor and outdoor air pollution, the demand for gas sensor is also rising globally and various types of gas sensors such as optical [5-6], electrochemical [7-8], semiconducting [9-11] and FET-type [12-14] gas sensors have been widely reported so far. However, most of the studies on gas sensors have been focused on semiconducting gas sensors which are resistor-types in general [9-11] and the investigation of sensing materials [15-17]. Most of the semiconducting gas sensor currently in production are a resistor-type having a semiconductor sensing

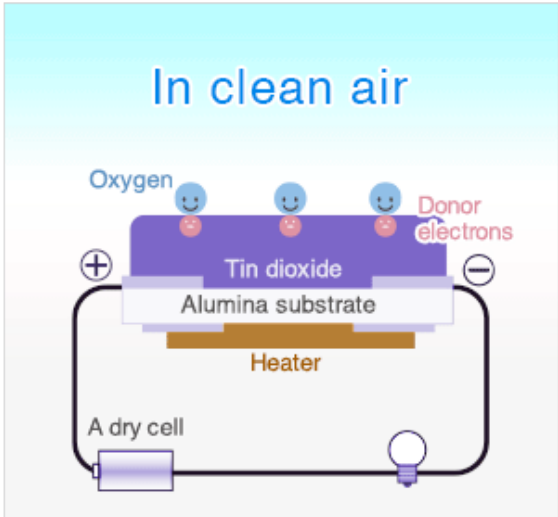

Fig. 1.1 Semiconducting gas sensor currently being produced by FIGARO, Japan.

layer between two electrodes (Fig. 1.1). It has a small size and consumes a low power compared to optical and electrochemical gas sensors [5]. However, it has a drift problem and its manufacturing yield is relatively low [5], [9]. Furthermore, it still has demerits in size and integration with CMOS circuits [18]. On the other hand, although the FET-type sensors have a higher degree of freedom coming from four terminal features in enhancing the sensing performance, fewer studies about FET-type gas sensors have been carried out than those about any other types of gas sensors mentioned above. There are two kinds of conventional FET-

type gas sensor reported so far. One is a thin film transistor (TFT) gas sensor which has a semiconducting sensing layer used as a channel of FET [12], [19]. When the sensing layer is exposed to a target gas, specific reaction will directly cause a change in conductance of the channel. This sensor is more sensitive than semiconducting gas sensor owing to its tunability of the conductance of conductive channel by controlling the gate voltage [13], but still has low production yield [14]. The other is a Si-based hydrogen (H_2) sensor having palladium (Pd) or platinum (Pt) gate [20-21]. H_2 gas molecules can penetrate porous Pd or Pt gate and form a dipole layer at gate-SiO_2 interface. A work function (WF) of the gate is changed by the dipole layer and therefore H_2 gas can be detected [20-21]. By using standard CMOS fabrication technology, this H_2 sensor has a smaller size [21] and a higher manufacturing yield [22] than semiconducting gas sensor. However, it is difficult for the H_2 sensor to detect various target gases having large molecules since gas molecules which are much larger than H_2 molecule can hardly permeate the porous gate.

To solve this problem, a Si FET-type gas sensor can be the good candidate

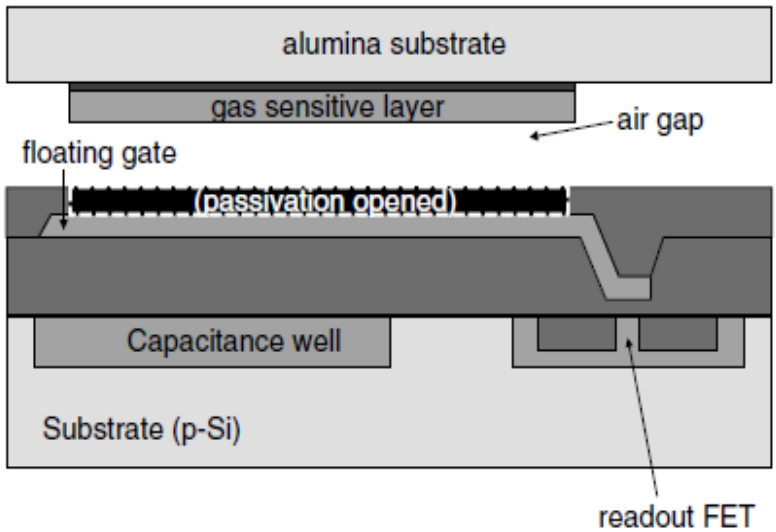

Fig. 1.2 Si FET-type gas sensor having a suspended gate structure. There is an air gap between the control gate and the floating gate, and a sensing layer formed right below the CG [23].

for the gas sensor. A Si FET-type gas sensor having suspended gate structure has been developed as shown in Fig. 1.2 [23-26]. Because it features an air gap between the control gate (CG) and the floating gate (FG), and a sensing layer formed right below the CG, a diversity of sensing materials can be applied and various gases can be detected as a result. However, this sensor having the air gap inside the device has structural instability. Moreover, the coupling ratio between

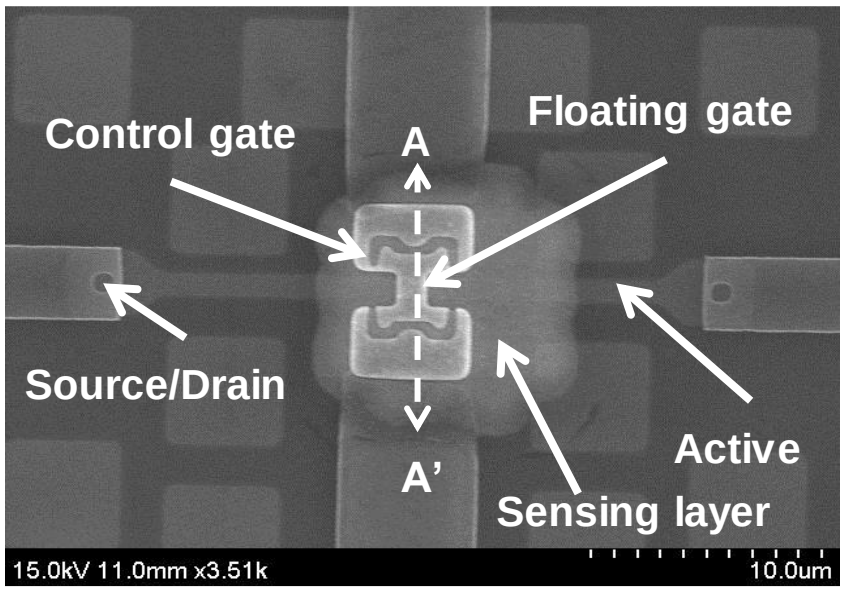

Fig. 1.3 C.H. kim *et al.* reported the Si FET-type gas sensor having a floating gate [27].

the CG and the FG decreases due to a small dielectric constant (ε_r) of air (ε_r = 1.00) so that the device performance is degraded. To compensate low coupling ratio, the size of the device has to be larger.

Thus, we have already proposed a new metal-oxide-semiconductor field-effect transistor (MOSFET)-based gas sensor having a FG which is horizontally formed next to a CG as shown in Fig. 1.3 [27-28]. The MOSFET-based gas sensor is fabricated by using standard CMOS technology so that the device size

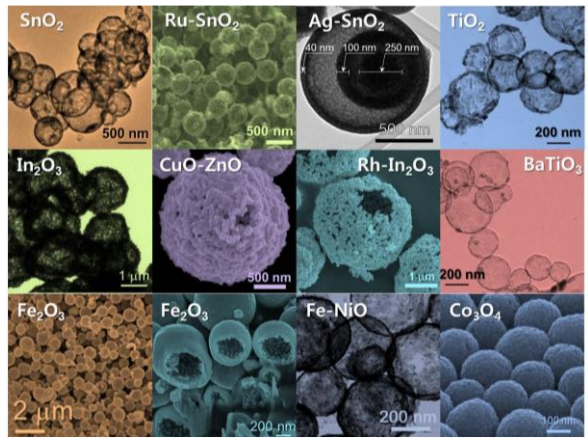

Fig. 1.4 Various types of metal oxide hollow spheres for gas sensing material reported by Prof. J.H. Lee's research group [38].

can be minimized and its manufacturing yield is high. Since a sensing layer is deposited at the final step of device fabrication, this gas sensor can monitor various target gases with diverse sensing materials. In addition, since several fingers of the FG are interdigitated with the CG in the horizontal direction, the gas sensor exhibits a good performance with a high coupling ratio [27-28].

Various types of sensing material such as carbon material [29-30], 2D material [31-32], metal oxides [33-36], solid electrolytes [37], and etc. have been studied in many research groups. Among them, to increase the response the gas

sensor, researchers are focused on nano-structured material with a variety of materials [35]. By using the metal oxide, various oxide hollow spheres, oxide hierarchical nanostructures, oxide nanowires are studied by J.H. Lee's research groups [38]. In addition, to increase the selectivity of the gas sensor, by decorating the metal catalyst such as Pt, Pd, Rh, and Au on carbon nanotubes, A. Star *et al.* demonstrated the gas sensor array that can detect several gases [39]. However, these techniques for enhancing the sensing performance have low yield, stability, reliability, and hard to combine with FET-type gas sensor due to its fabrication process. Thus, to enhancing the sensing characteristics in FET-type gas sensor, more studies are needed.

1.1.2 Improvement of gas sensing characteristics

Recently, to improve gas sensing characteristics, two kinds of techniques have been used, which are UV illumination and heating effect [40-43]. The electrons supplied by UV or heat enhance the adsorption and desorption of gas molecules. S. Zhang *et al.* reported the excess photo generated electrons are

increase the adsorption of the oxygen molecules. In addition, the heating effect of the FET-type gas sensor having ZnO film as a sensing layer is reported in our previous research. Y. Hong *et al.* reported that transient I_D behaviors are measured at 20 ppm of NO_2 gas as a parameter of the temperature from 25 ^oC to 180 ^oC. As the temperature increases, the response time and the recovery rate is significantly decreased [28]. The increased kinetic energy of NO_2 molecules and excess electrons in ZnO film by high temperature increase the gas response and recovery properties. However, these two methods need bulky equipment such as external light source and heater, which is difficult to apply to the practical gas sensor.

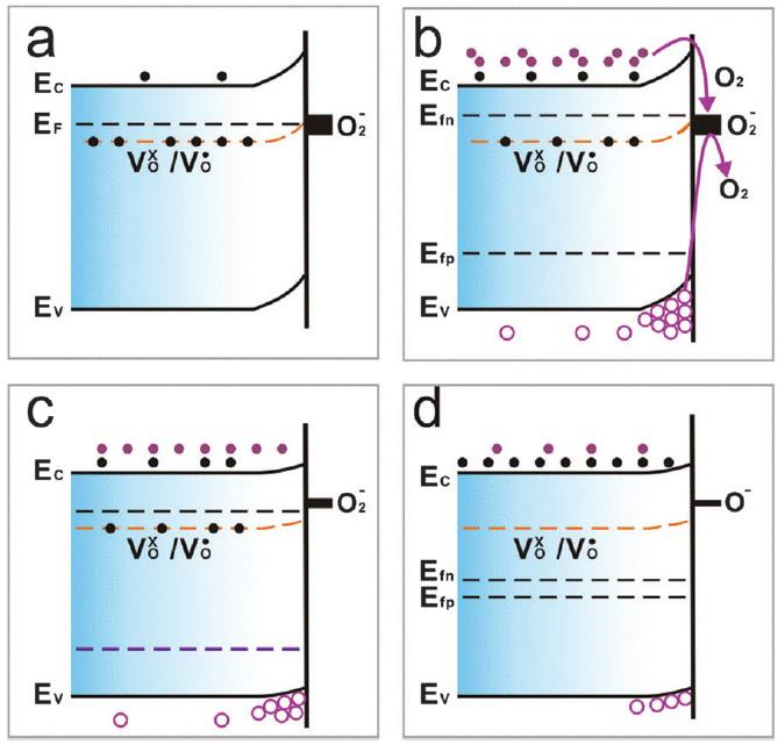

Fig. 1.5 Enhancement gas adsorption and desorption by UV illumination [41].

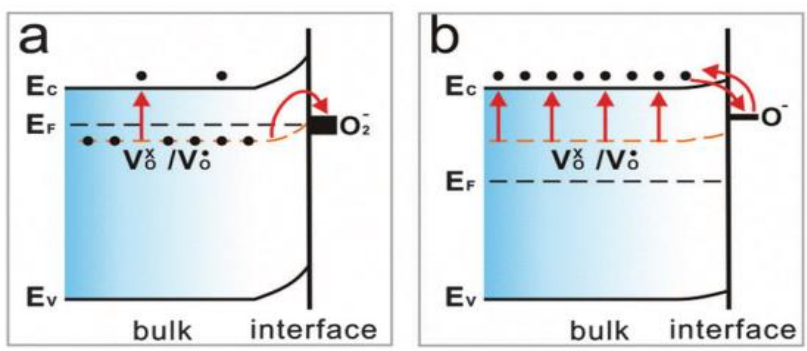

Fig. 1.6 The heating effect [41].

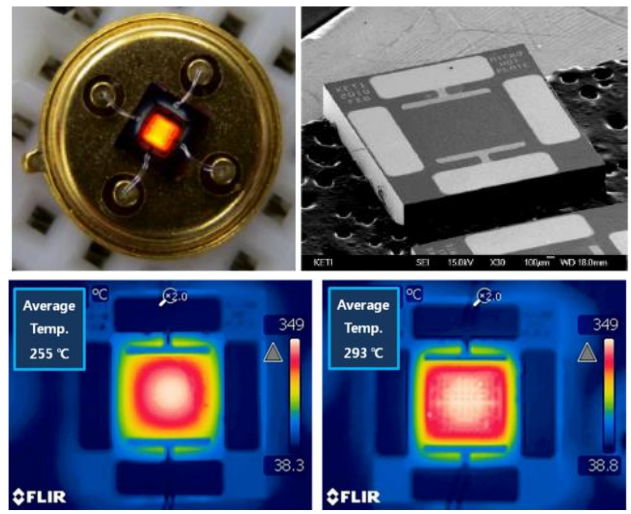

Fig. 1.6 Embedded micro-heater in the resistor-type gas sensor [42].

1.2 Purpose of research

Although the FET-type sensors have a higher degree of freedom coming from four terminal features in enhancing the sensing performance, there have been no report on electrical control scheme. In this paper, we investigate, for the first time, the pre-bias effect on the response and recovery characteristics of Si FET-type gas sensor. A new pulse bias scheme for the pre-bias (V_{pre}) is devised to increase gas response and to reduce recovery time. We analyze the reaction between NO_2 gas and the ZnO sensing layer deposited on the Si FET-type gas sensor.

1.3 Thesis outline

Based on the Si FET-type gas sensor having the CG and the FG in horizontal direction, this work is mainly focused on the pulse pre-bias effect. In Chapter 2, the structure and the key fabrication process of the FET-type gas sensor are briefly described and the issues for the fabrication are explained in detail. In Chapter 3, the measured electrical characteristics of the fabricated *p*MOSFET gas sensor are shown and the electrical modeling of the sensor are explained. In addition, the sensing mechanism of FET-type gas sensors are explained specifically. In Chapter 4, the pulse pre-bias scheme is proposed to increase the gas response and recovery characteristics. The gas response and recovery characteristics are measured as a parameter of the pre-bias and the mechanisms responsible for the pre-bias are explained by energy band diagram. The advantages of the pre-bias effect are explained and the considerations for the pulse pre-bias scheme are discussed. Chapter 5 concludes this dissertation with a summary. The researches about various types of sensors are discussed in Appendices.

Chapter 2

Device structure and fabrications

2.1 Device Structure

The structure of the Si FET-type gas sensor which has a floating-gate (FG) and a control-gate (CG) facing each other in horizontal direction is shown in Fig. 2.1. By using only 5 mask steps, Si FET-type gas sensor can be fabricated including sensing layer. The top SEM image of the fabricated FET-type gas sensor is shown in Fig. 2.1 (a). As a sensing layer, the ZnO film covers a part of CG and the passivation formed on the FG as represented by a white dashed line in Fig. 2.1 (a). Surface SEM images of the ZnO layer formed on SiO_2 (top) and the FG (bottom) covered by insulating stack in Fig. 2.1 (b). Fig. 2.1 (c) shows a schematic cross-sectional view of the fabricated FET-type gas sensor cut along a dotted line A-A' is shown in Fig. 2.1 (a). Fig. 2.1 (d) shows a schematic cross sectional view of the fabricated FET-type gas sensor cut along a dotted line B-B' in channel direction. Most of fabrications for gas sensors were implemented with the facilities of Inter-university Semiconductor Research Center (ISRC) at Seoul

National University and National Nano-Fab Center (NNFC) located at Daejeon.

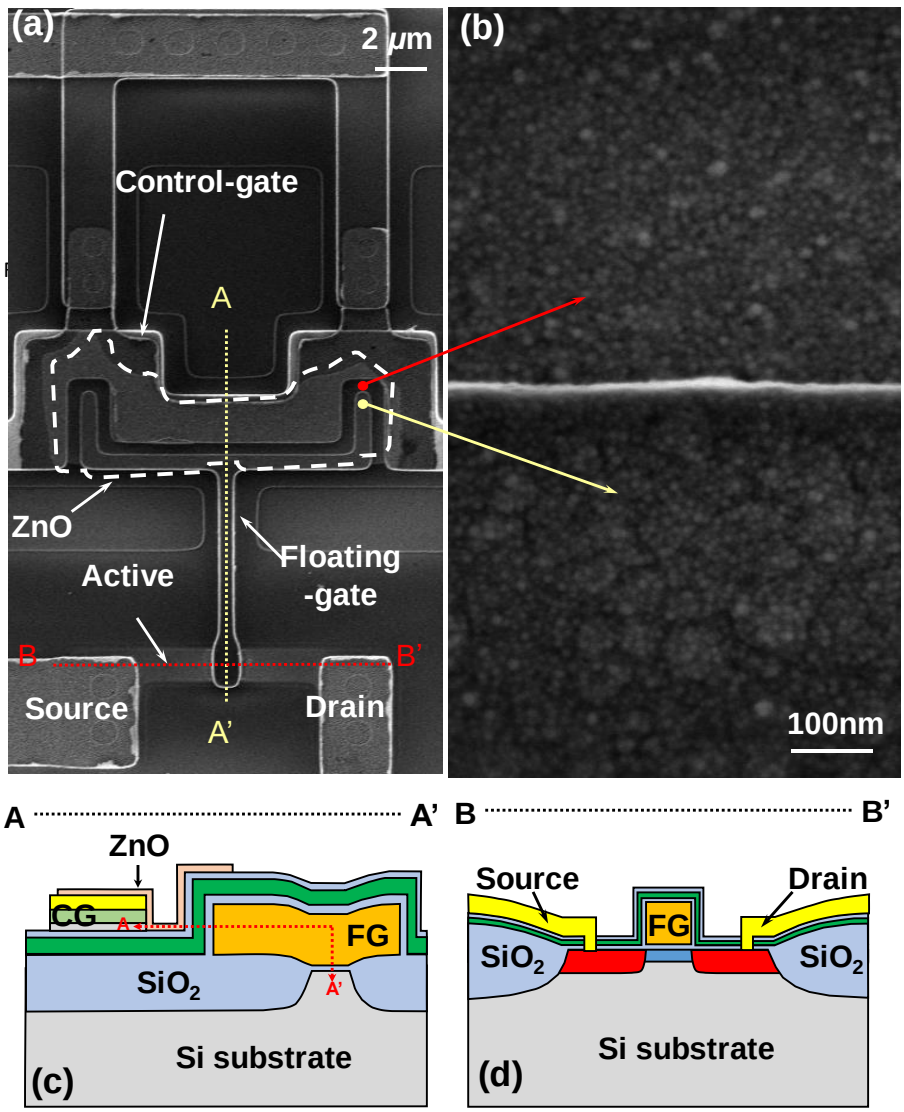

Fig.2.1 (a) Top SEM image of the fabricated FET-type gas sensor. (b) Surface SEM views of the ZnO layer formed on SiO_2 (top) and FG (bottom). Schematic cross-sectional view of the fabricated FET-type gas sensor cut along the yellow dashed line A-A' (c) and the red dashed line B-B'(c).

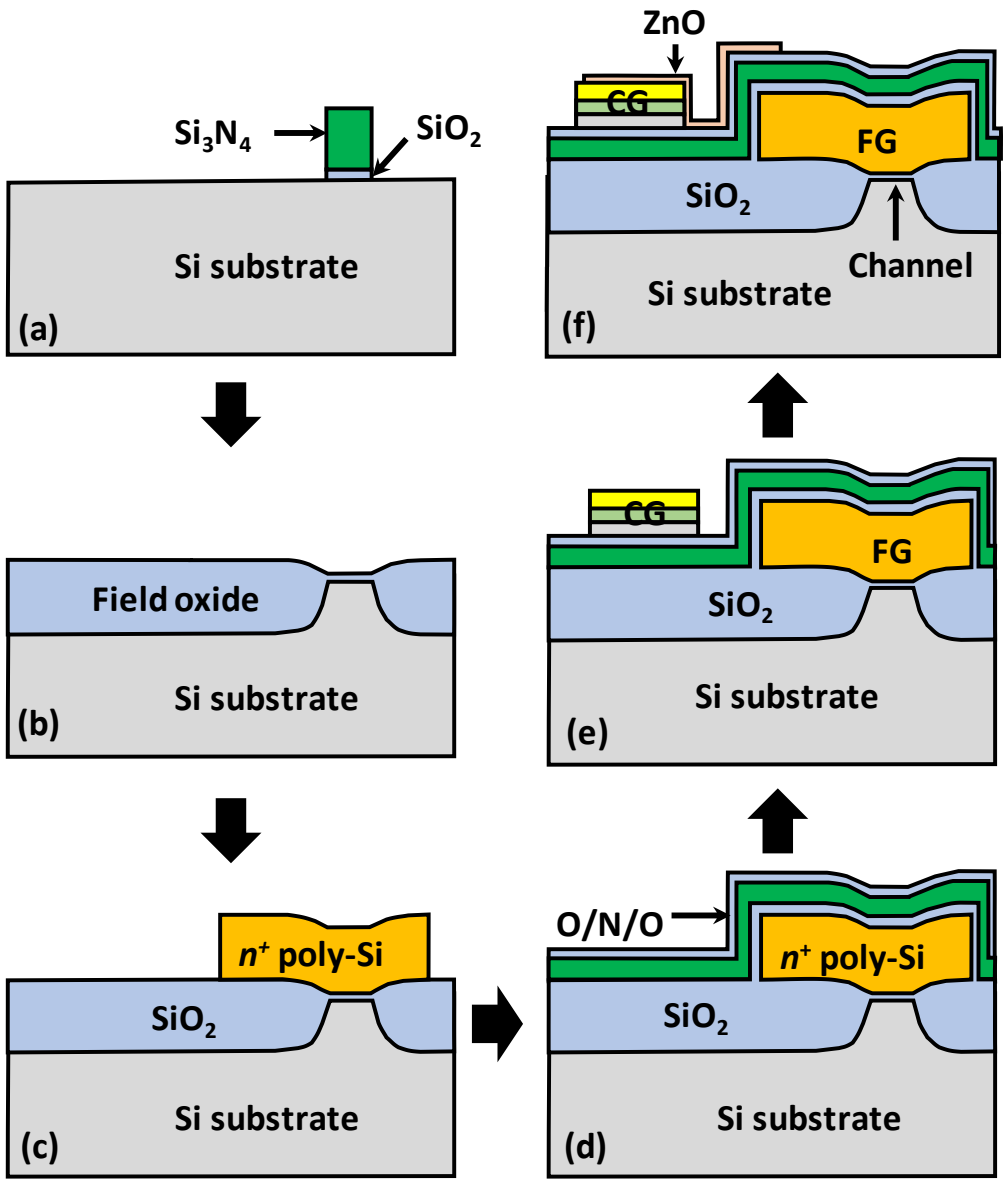

Fig.2.2 Schematic cross-sectional views of key fabrication process steps of the FET-type sensor cut along a yellow dashed line A-A' in Fig. 2.1 (a). By using five mask steps, the FET-type gas sensor can be fabricated including sensing layer.

2.2 Device Fabrication

2.2.1 Key fabrication process

Schematic cross-sectional views of key fabrication process steps of the FET-type gas sensor are shown in Fig. 2.2. Starting substrates are 6 inch single crystalline Si wafers having (100) orientation. Half of the total number of wafer is *p*-type(5~10 Ω·cm) and the other half is *n*-type (1~10 Ω·cm). After typical silicon wafer cleaning process which include SPM (H_2SO_4+H_2O_2), SC-1 (H_2O_2+NH_4OH+H_2O), SC-2 (H_2O_2+HCl+H_2O), and HF, 10 nm of pad oxide is thermally grown in dry oxygen ambience and 150 nm of silicon nitride (Si_3N_4) layer is deposited by using a lower pressure chemical vapor deposition (LPCVD) method. Both layers defined by photoresist (PR) patterning using active mask (1^{st} mast) and dry etch process (Fig. 2.2 (a)). And then, 550 nm thick field oxide is grown at 1000 ^oC for 2 hours by using wet oxidation process for the isolation of active regions (Fig. 2.3 (a)). Here, the silicon uncovered by the Si_3N_4 patterns is selectively oxidized and this step is called Local Oxidation of Silicon (LOCOS) process. Since the silicon oxynitride is formed on the Si_3N_4 during the

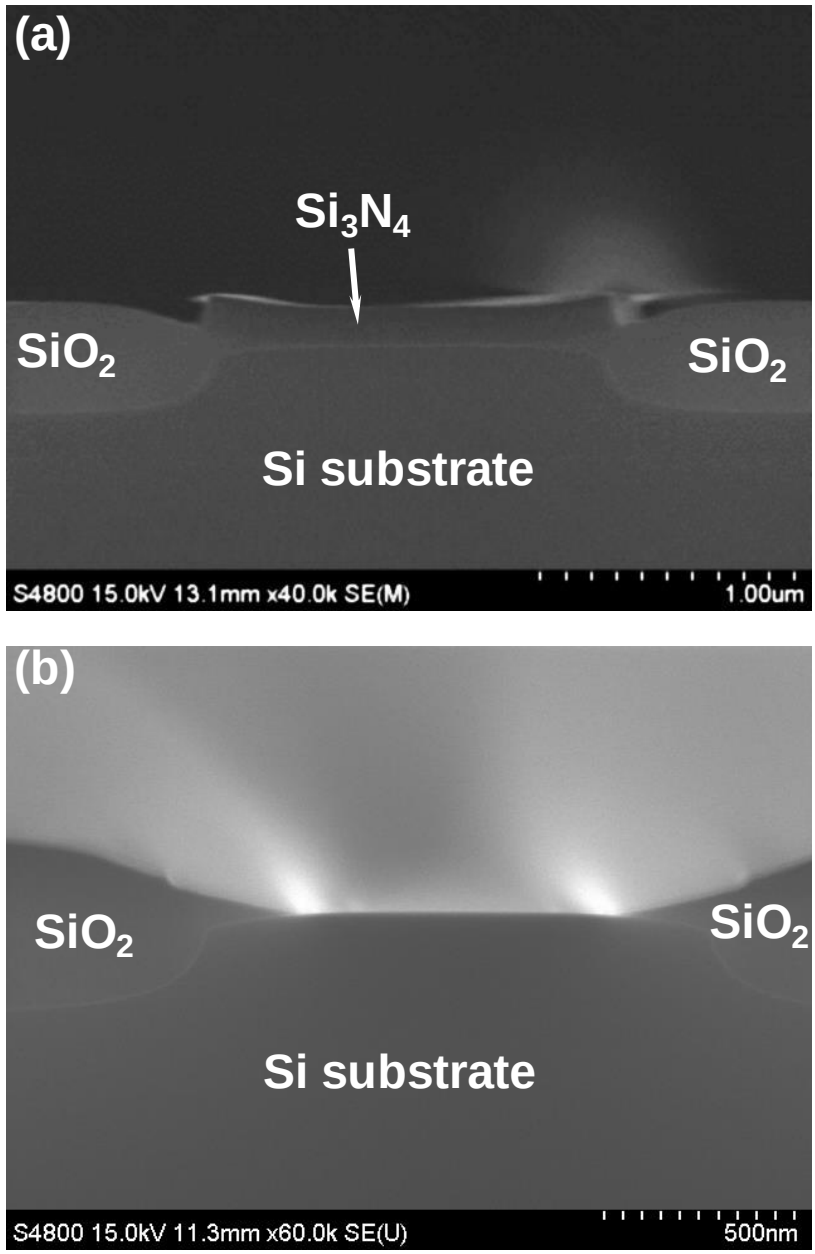

Fig.2.3 (a) SEM images of the active region of the MOSFET after growing the field oxide and (b) define active region after etching Si_3N_4 and pad oxide.

wet oxidation process, the silicon oxynitride film is firstly removed by an HF solution. Then, the Si_3N_4 layer is stripped in H_3PO_4 solution at 160 ºC and the pad oxide is etched in an HF solution (Fig. 2.2 (b)). The defined active region by LOCOS process is shown in Fig. 2.3 (b). In order to remove the white ribbon generated during the LOCOS process, 30 nm thick sacrificial oxidation is carried out [44]. Then, 30nm of oxide is etched by HF leaving a 10 nm thick sacrificial oxide for channel implantation. The *p*MOSFET sensor is mainly fabricated because it has lower 1/f noise than the *n*MOSFET [45]. Consequently, the *p*MOSFET sensors and MOSFETs of the peripheral circuits composed of the *p*MOSFET are simultaneously fabricated without *n*MOSFET through same fabrication process, and the number of masks can be reduced. BF_2^+ ions for the *p*MOSFET sensor are implanted to implement a buried channel which guarantees low 1/f noise and control the *V*th of the *p*MOSFET sensor [46]. To compare with buried channel MOSFET, P^+ ions implantation which is conventionally used in *p*MOSFET are also conducted to fabricated surface channel device. The channel implantation is more deeply mentioned in Ch. 2.2.2.

Rapid Thermal Process (RTP) for activation and diffusion of implanted ions is then conducted at 1050 ºC for 5 seconds. The 10 nm of sacrificial oxide etched in an HF solution. 10 nm thick gate oxide is grown by using dry oxidation process at 800 ºC to protect thermal budget. A layer of *in situ* doped n^+ poly-crystalline Si is deposited with a thickness of 350 nm at NNFC. The poly Si is patterned to form the FG for the MOSFET sensor platforms and the gate electrodes for the MOSFET in peripheral circuits (Fig. 2.2 (c)). Then ion implantation by BF_2^+ ions with a dose of 2×10^{15} cm^{-2} is carried out to form the source and drain in self aligned manner using the patterned poly Si as a hard mask for the implantation. As followed by ion implantation, RTP for activation and diffusion of implanted ions is then conducted at 1050 ºC for 5 seconds. Since the Si_3N_4 layer is applied to protect from molecules (such as ions and water molecules) from penetrating in to the FG and channel, Si_3N_4 is formed as a passivation layer. Since the formation of the 10 nm thick oxide layers above and below the Si_3N_4 are carried out to avoid unwanted charge trap at the interface between the Si_3N_4 layer and a sensing layer, an O/N/O passivation consisting of

SiO_2 (10 nm)/ Si_3N_4 (20 nm)/ SiO_2 (10 nm) layers is formed on the wafers (Fig. 2.2 (d)). After defining the contact holes by RIE etch, PR patterning for a lift off process is followed by the consecutive deposition of Cr (30 nm) and Au (50 nm) using sputtering process. By removing the PR by acetone, the electrode for the CG, source, and drain are formed at the same time (Fig. 2.2 (e)). And then, hydrogen (H_2) annealing for improving the contact property is conducted at 300 ^oC for 10 min. Finally, a sensing layer is formed around the FG and CG facing each other through the patterning (Fig. 2.2 (f)). Since the formation of the sensing layer is the final step of the fabrication process, various sensing materials sensitive to gases can be used as a sensing layer. Moreover, since the sensing layer is covered a part of O/N/O passivation on FG, the sensing layer which is electrically contacted to CG electrode acts as a CG of the FET-type gas sensor.

2.2.2 Simulation study for buried channel implantation

The buried channel implantation was introduced to control the threshold voltage (V_{th}) as well as lower 1/f flicker noise characteristics. To estimate experimental result more accurately, a process simulation tool (Silvaco Inc. Athena) is conducted. To allow MOSFETs in peripheral circuits to operate in the enhancement mode (normally off), V_{th}s of the MOSFET must be higher than 0 V. Also, the n^+ doped poly Si is used for gate of the *p*MOSFET, *V*th of the *p*MOSFET is quite high. Thus, BF_2^+ ions implantation is used for controlling the *V*th while reducing 1/f noise. Fig. 2.4 shows the simulated transfer characteristics as a parameters of BF_2^+ ion dose (/cm^2) from 1.4×10^{12} to 6.0×10^{12} with power of 25keV. As the dose of BF_2^+ ion increases, the *V*th of *p*MOSFET decreases. When a dose of BF_2^+ is higher than 4.0×10^{12}, the off current (I_{off}) is increases. Fig. 2.5 shows the measured I_D-V_{GS} curves of the fabricated *p*MOSFET as a parameter of BF^{2+} ion dose. The surface channel implantation which is implanted by P^+ ion is fabricated as a reference. Considering a V_{th} and I_{off}, the buried channel implantation is performed with a

BF_2^+ dose of 2×10^{12}.

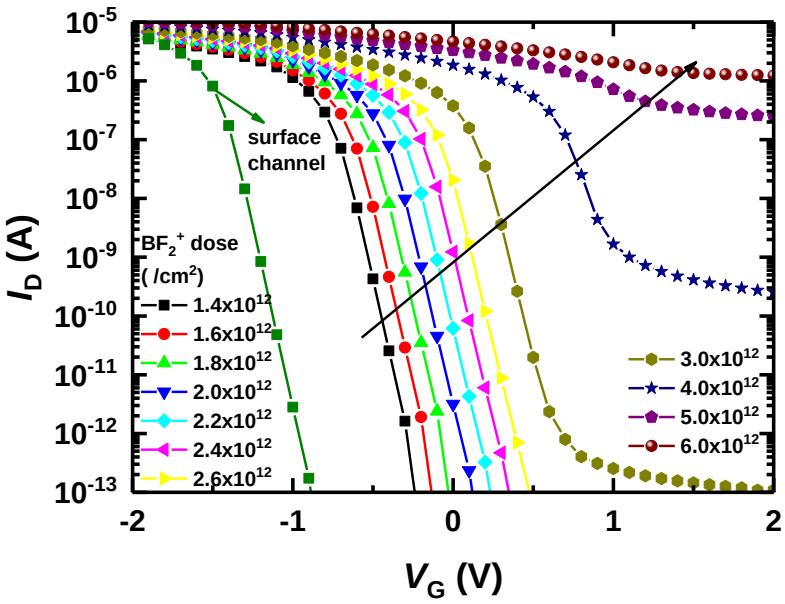

Fig.2.4 Simulated I_D-V_G curves as a parameter of BF_2^+ ion dose.

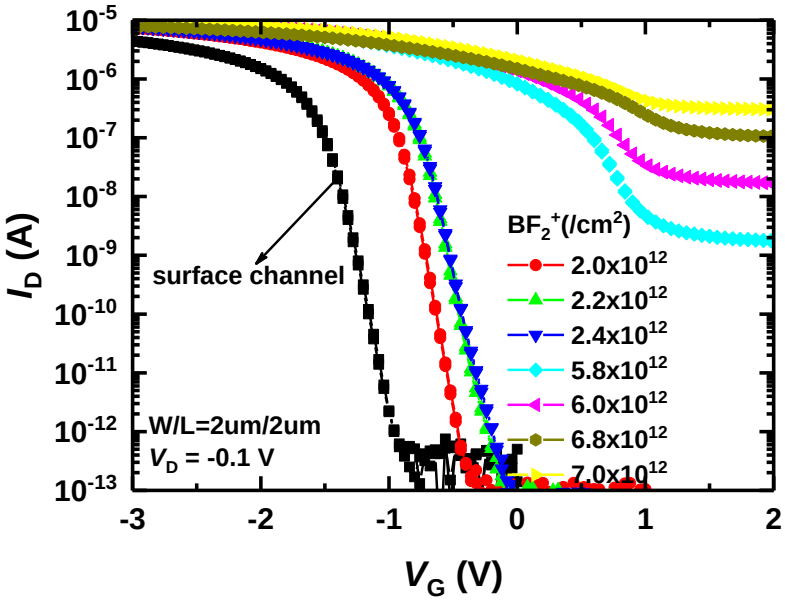

Fig.2.5 Measured I_D-V_G curves of the fabricated MOSFET as a parameter of BF_2^+ ion dose.

2.2.3 Formation of sensing material

In the FET-type gas sensor, the CG and FG formed horizontally face each other, and a sensing layer is formed between CG and FG so that the channel of the *p*MOSFET sensor and the sensing area are formed apart in the horizontal direction. However, most of gas sensitive materials such as metal oxides [47-49], carbon materials [50-52], 2D metal dichalcogenides (TMDCs) [32,39], etc. are not CMOS compatible [53]. Therefore, to protect MOSFET from the contamination during the formation of sensing layer, a sensing layer is formed in the final step of fabrication process.

Three typical methods for forming a gas sensitive material have been used in our research such as atomic layer deposition (ALD) [28,54], sputtering [55,56] and inkjet printing method [57,58]. Firstly, among them, to reduce the mask steps, inkjet printing method is used. The inkjet printing method has advantages such as good patterning capability, low cost, and easy to combine with various sensing material in sensor array without patterning process. Solution type of nanomaterial such as SWNTs, metal oxides, TMDCs is widely

used. SWNTs was adopted in FET-type sensor for sensing layer [58]. However, the device to device variation and poor contact with CG electrodes limit the reliable sensing characteristics. On the other hand, the physical vapor deposition (PVD) method such as sputtering and ALD has the disadvantage that the same sensing material is formed on the FET-type sensors and one more mask step is needed. However, due to uniform deposition and good contact property between CG electrodes and sensing material, PVD methods such as sputtering and ALD is widely used. Among them, since the ALD can uniformly deposit even thin film such as several nm, the sensing layer formed by ALD is appropriate for analyzing the sensing characteristics in FET-type gas sensor [54-56].

Therefore, in this research, the ZnO film is used as a sensing layer by ALD. The ZnO film is grown by ALD using diethylzinc (DEZn) and ozone (O_3) as a Zn precursor and an oxidant, respectively, at 250 ^{o}C. By using the X-ray photoelectron spectroscopy (XPS), we observe Zn2p3 peak (1022.08 eV) and O 1s peak (532.08 eV) which are consistent with the reported value from ZnO film as shown in Fig. 2.6. The thickness of ZnO film is 15 nm.

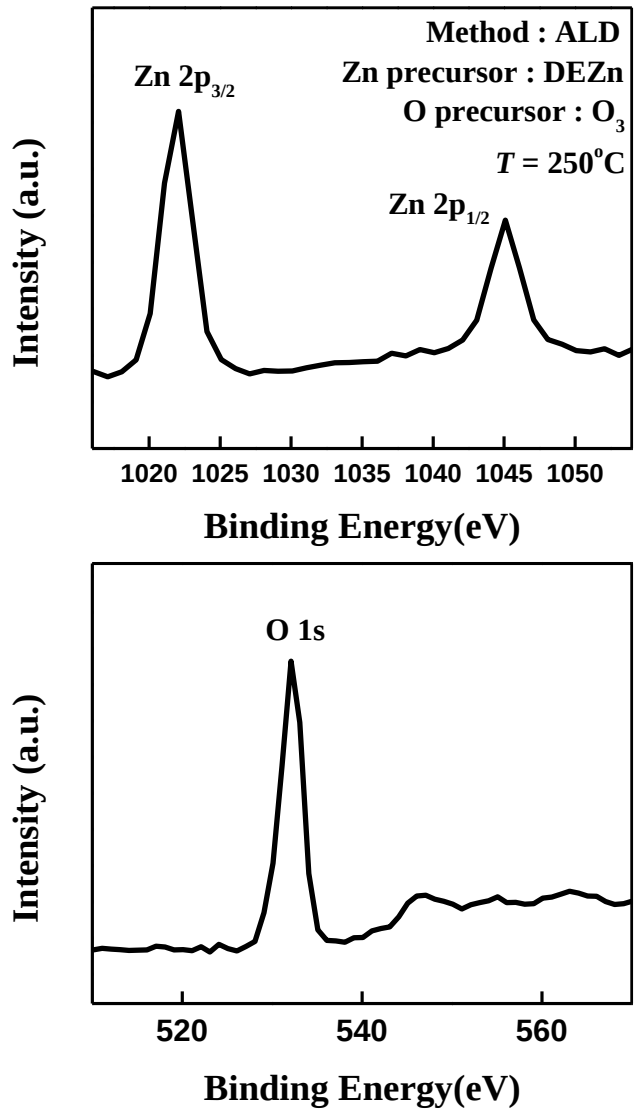

Fig. 2.6 XPS survey spectra of ZnO. The ZnO as a sensing layer is deposited by ALD. The formed ZnO film shows a peak of Zn2p3 (1022.08 eV) and O 1s (532.08 eV) which is consistent with the reported value of ZnO.

Chapter 3

Device characteristics

3.1 *I_V* characteristics of FET-type gas sensor by DC and PIV method

The *I_V* characteristics of *p*MOSFET gas sensor have been conducted by DC and pulsed *I_V* (PIV) method using a semiconductor parameter analyzer (B1500A, Agilent). The pulsed *I_V* measurement is carried out using Waveform Generator/Fast Measurement Unit (WGFMU) measurement system based on Agilent B1500. The pulse wave form used for the PIV is depicted in Fig. 3.1. The control-gate read bias (V_{rCG}) and base voltage (V_{base}) is alternatively applied to the CG having pulse widths of t_{on} of 50 μs and t_{off} of 100 ms, respectively. The drain read pulse (V_{rDS}) is synchronized with the V_{rCG}. By reducing t_{on} as short as possible and applying the V_{base} of 0 V to the CG, the DC stress to the sensor can be minimized, resulting in the removal of I_D drift and hysteresis of I_D-V_{CG} curves.

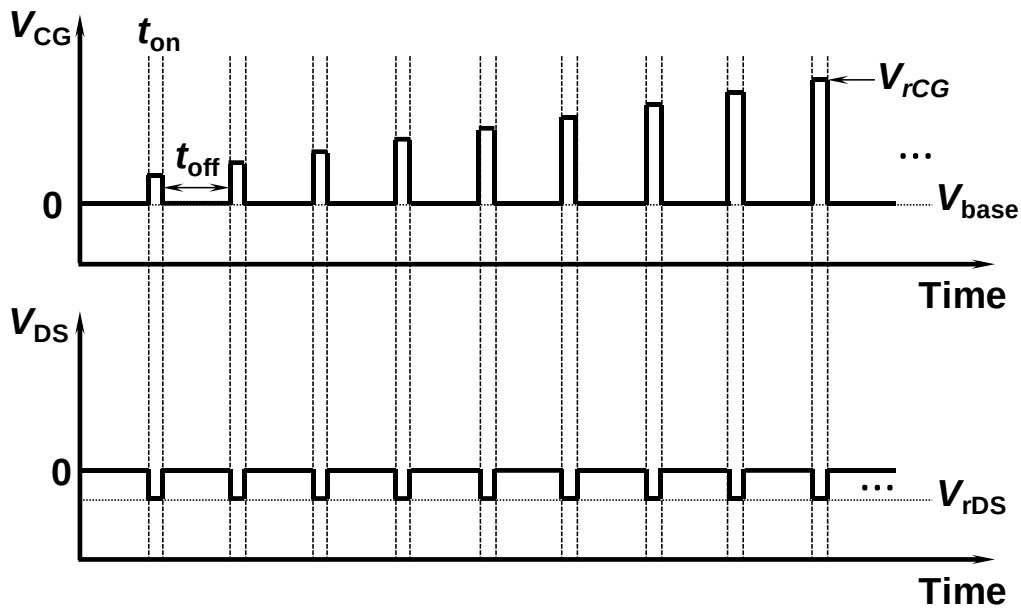

Fig. 3.1 The pulse wave form for the PIV

The transfer (I_D-V_{CG}) and output (I_D-V_{DS}) characteristics of the *p*MOSFET sensor are measured by DC and PIV as a parameter of temperature (Fig. 3.2 (a) and (b)). The width and length of the channel of the *p*MOSFET sensor is 2 μm and 1μm, respectively. The V_{rDS} is fixed at -0.1 V. As the temperature increases from 20 ^{o}C to 220 ^{o}C, the off-current of I_D-V_{CG} curves increase due to drain to substrate junction leakage current [59].

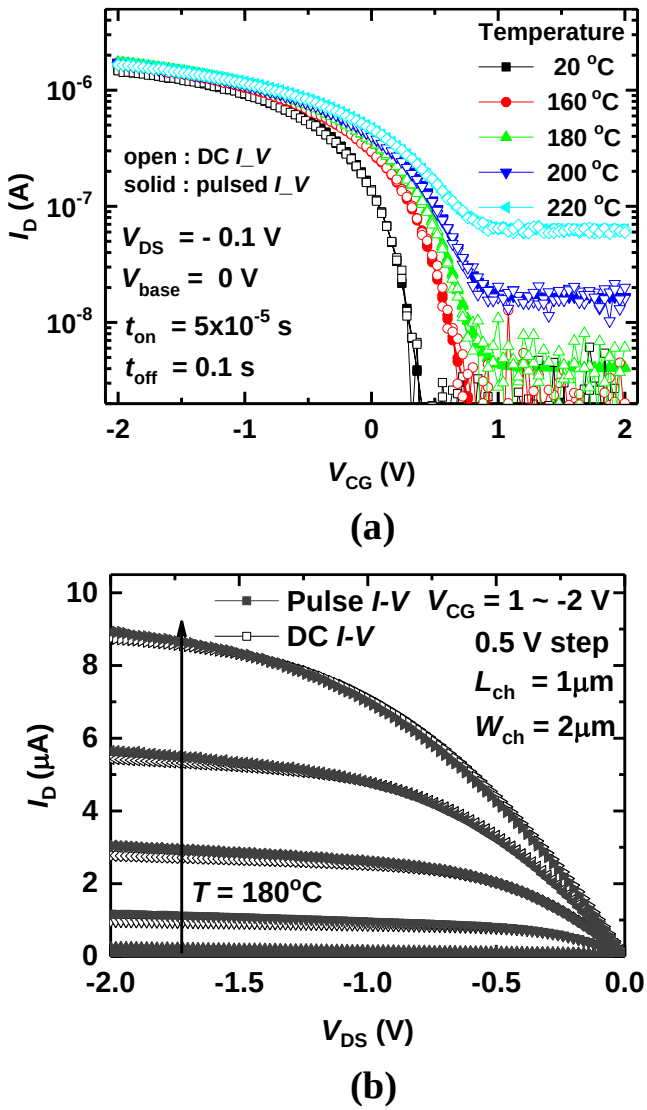

Fig. 3.2 (a) Transfer (I_D-V_{CG}) curves of the *p*MOSFET sensor measured by the DC and PIV methods as a parameter of T (20 °C, and 160-220 °C) at V_{DS} = -0.1 V. (b) Output characteristics of the *p*MOSFET sensor measured by the DC and PIV methods at T = 180 °C.

3.2 Electrical modeling of the FET-type gas sensor

The equivalent circuit of the gas sensor is represented in Fig. 3.3 (c) along a red dotted line A-A' in Fig. 3.3 (a). Since the ZnO as a sensing material is formed in the last process step to avoid contamination, it is deposited after forming the CG. Therefore, the ZnO is directly attached on the CG electrode. The CG can be divided into three parts. ① which is represented by green dashed line in Fig. 3.3 (b) is a junction between the CG electrode and the ZnO. ② which is represented by yellow dashed line in Fig. 3.3 (b) is a bulk region of the ZnO. In other words, ② is un-contact area of the ZnO. ③ which is represented by red dashed line in Fig. 3.3 (b) is an interface between the ZnO and O/N/O stack.

Firstly, the ZnO and CG form the metal-semiconductor junction. Depend on the work-function of both material, they form the Schottky or ohmic contact, which is modeled by parallel resistor and capacitor represented in the Fig. 3.3 (c). R_C and C_C are the contact resistance and capacitance, respectively. Since the ZnO deposited by ALD at 250 ^oC, in this research, is reported that it has high electron conductivity, the ZnO and CG form the ohmic contact. Thus, even

though the work-function of the ZnO and Au as a CG is 4.3 eV and 5.1 eV, the parallel R_c and C_c can be simplified by a resistor.

Because of the O_2 adsorption at working temperature which is 180 ^oC, the grains of the ZnO are depleted, resulting in band bending at the interface of the grain [60]. The bulk region of the ZnO which is represented by yellow dashed line in Fig. 3.3 (b) is modeled by parallel resistor and capacitor represented in the Fig. 3.3 (c). The R_{ZnO_B} and C_{ZnO_B} are the contact resistance and capacitance, respectively. Since the carrier concentration of the ZnO in this research is high, the C_{ZnO_B} can be ignored. Thus, the parallel R_{ZnO_B} and C_{ZnO_B} can be simplified by a resistor.

Finally, the interface between the ZnO and O/N/O stack is modeled as parallel capacitors, C_{gas} and C_{int}. Since the CG and the ZnO are electrically connected, the potential of the ZnO is equal to the CG. Thus, most of band bending occurs at the interface between the ZnO and O/N/O stack. Depend on the bias of the CG, depletion region of the ZnO is changed resulting in the change of the capacitance at the interface. This capacitance is denoted by C_{int}. In

addition, since the capacitance of the interface is significantly changed by gas adsorption, this capacitance is denoted by C_{gas}.

By simplifying the CG part, a modified equivalent circuit of the FET-type gas sensor is shown in Fig. 3.3 (d). As mentioned above, due to the high concentration of the ZnO, R_C and R_{ZnO_B} is substituted by R_{CG}, and parallel capacitance, C_{int} and C_{gas} can be substituted by C_{CG}. Therefore, the CG part is simply modeled by series resistance and capacitance, which are R_{CG} and C_{CG}. The coupling ratio (γ) of the FET-type gas sensor is

$$\gamma = \frac{(C_{CG} \,/\!/\, C_{ono})}{(C_{CG} \,/\!/\, C_{ono}) + C_g + C_p} \tag{1}$$

, where the C_{CG}, C_{ono}, C_p, and C_g denote the capacitances of the CG, the O/N/O passivation stack, the parasitic, and gate oxide capacitances, respectively. By adopting the interdigitated structure in CG and FG, the coupling ratio can be increased.

To apply the appropriate pulse to the FET-type gas sensor, RC delay should be considered. However, it is difficult to measure the resistance and capacitance exactly. Considering the size of the ZnO, the R_{CG} is approximately calculated

from the *I-V* curve of the resistor type gas sensor (Fig. 3.7). The R_{CG} is approximately 233 MΩ. Since the doping concentration of the ZnO is high, the C_{CG} is much higher than C_{ono}, C_p, and C_g. By ignoring the C_{CG}, total capacitance of the FET which include C_{ono}, C_p, and C_g is about 6.79 fF, in air ambience. Thus, the RC delay of FET-type gas sensor having a ZnO as a sensing layer is about 1.51μs. To calculate the RC delay accurately, the exact value of resistance and capacitance should be considered. Thus, further study is needed for extracting RC time constant exactly.

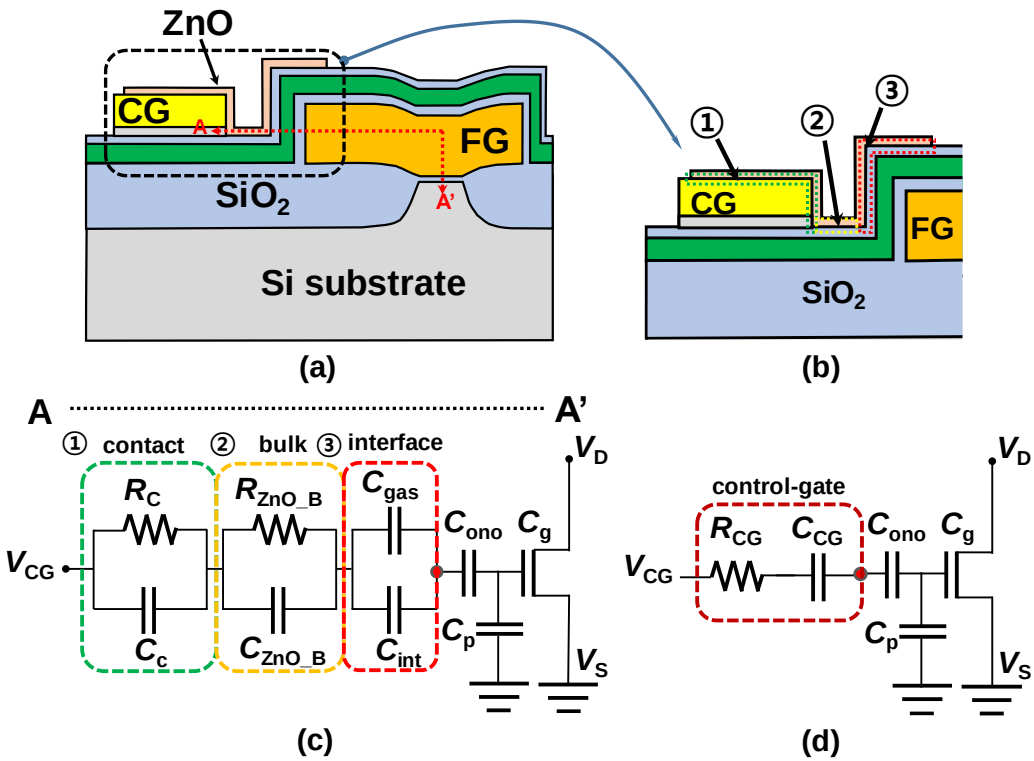

Fig. 3.3 (a) Schematic cross-sectional view of the FET-type gas sensor. In this research, the ZnO is used as a sensing material. (b) Magnified region of the black dashed line in (a). The CG can be divided into three areas. (c) Equivalent circuit model of the gas sensor along a red dashed line A-A' in Fig. 3.3 (a). (d) Simplified equivalent circuit of the gas sensor.

3.3 Nonvolatile functionality

The gas sensor has a nonvolatile functionality by adopting the FG. To achieve the high coupling ratio, interdigitated FG and CG structures are fabricated. The variation of the I_D-V_{CG} curves under different program and erase biases (V_{PGM} and V_{ERS}) is shown in Fig. 3.4. The Si substrate of the device is grounded while the V_{PGM} and the V_{ERS} are both applied to the CG for 5 s simultaneously. The V_{th}s are increased by approximately 1 V and 2 V when the V_{PGM}s are -11 V and -12 V, respectively. On the other hand, the V_{th}s are decreased by roughly 0.6 V and 1.3 V when the V_{ERS}s are 11 V and 12 V, respectively. It is very important to note that the V_{th} of the sensor can be tuned by controlling the program and erase times (t_{PGM}, t_{ERS}), V_{PGM}, and V_{ERS}. The tunable V_{th} is very useful for calibrating the gas sensor and also changing the operating point of the load transistors in current to voltage amplifier. Fig. 3.5 shows excellent retention characteristics of the *p*MOSFET-type gas sensor at room temperature. In both the program and the erase states, negligible V_{th} shifts are observed for 10^4 s.

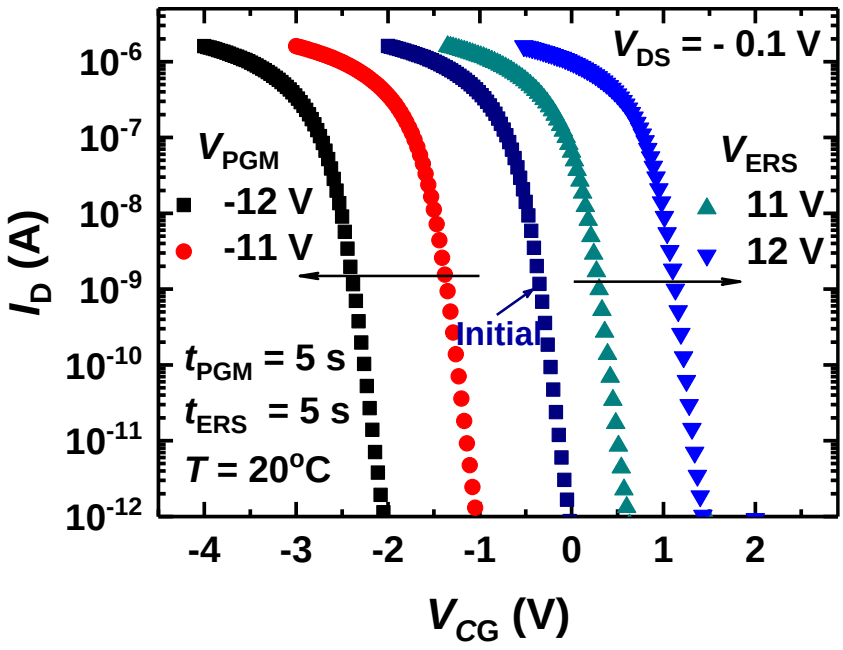

Fig. 3.4 Program and erase characteristics of the FET-type gas sensor as parameters of the program voltage (V_{PGM}) and erase voltage (V_{ERS}).

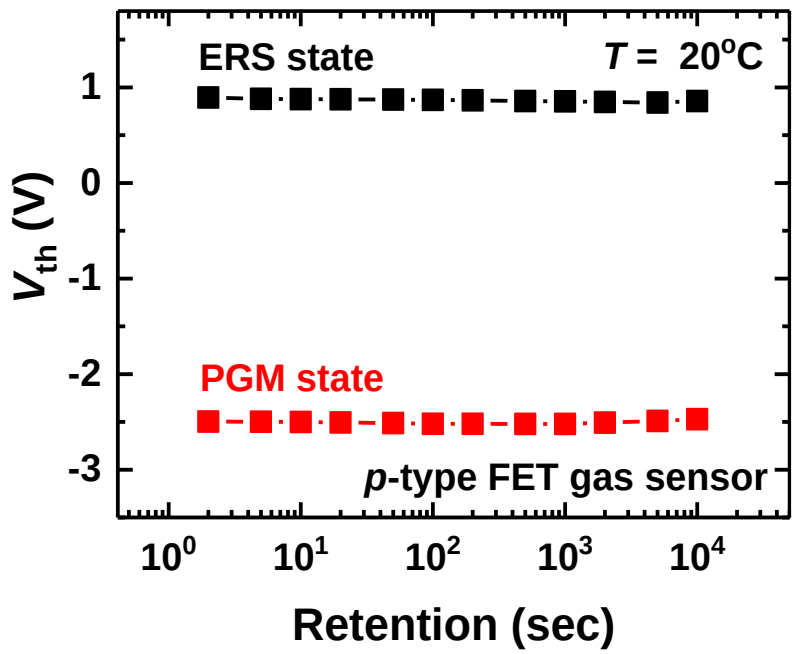

Fig. 3.5 Retention characteristics of the fabricated gas sensor. The V_{th} shifts are negligible up to 10^4 s.

3.4 Gas sensing mechanism of the FET-type gas sensor

There are two types of gas. The oxidizing gases such as NO_2, SO_2, CO_2, and etc. get electrons from the sensing material and are ionized. On the other hand, the reducing gases such as NH_3, H_2S, H_2, CO, and etc. loses electrons. The gas sensing mechanism is explained as follow. After the gas molecules reach the surface of the sensing material, they physically adsorb on the sensing material. Then, the chemical reaction between the gases and the sensing material occurs. Depend on the type of the gases, the conductance of the sensing material can be changed by the surface chemical process. In the case of the oxidizing gas such as NO_2, the free electrons in the conduction band of the sensing material are captured by the gas molecules, and the electrons near the surface of the sensing material are depleted. In contrast, the electrons are accumulated in the surface of the sensing material in the ambience of the reducing gas such as NH_3. Therefore, depending on the type of the gas, the work-function and capacitance of the sensing material which is a CG of the FET-type gas sensor are changed. The change of work-function of the sensing material changes the difference of the

work-function between gate and substrate, resulting in the change of the V_{th}. The V_{th} is defined by

$$V_{th} = \phi_{ms} - \frac{Q_{ox}}{C_{ox}} + 2\Psi_B + \frac{\sqrt{2\varepsilon_{si} q N_a (2\Psi_B + V_{BS}}}{C_{OX}} \quad (2)$$

In addition, the capacitance changes of the ZnO by gas reaction have an effect on the γ of the FET-type gas sensor. The change of the γ also affects the I_D.

Since the Si-FET type gas sensor have a FG, the drain current equations of the *p*MOSFET gas sensor are defined by

$$|I_D| = \mu C_g \frac{W}{L} (|\gamma V_{CG} - V_{th}| + \frac{1}{2}|V_{DS}|)|V_{DS}| \quad (3)$$

$$|I_D| = \mu C_g \frac{W}{L} \sqrt{\frac{\varepsilon_{si} q N_d}{4\Psi_B}} \left(\frac{kT}{q}\right) e^{-\frac{q(|\gamma V_{CG} - V_{th}|)}{mkT}} \quad (4)$$

in linear region and subthreshold region, respectively. Therefore, the change of V_{th} and γ by the gas molecule changes the I_D of the FET-type gas sensor. By changing the coupling ratio and work-function of the sensing material, gas molecules can be detected by the FET-type gas sensor.

Gas sensing characteristics of the FET-type gas sensor having a horizontal FG is conducted in our previous research by Y. Hong *et al*. [28]. In NO_2

ambience, the V_{th} of the *p*MOSFET gas sensor decreases. Because an NO_2 gas molecule extracts an electron from the ZnO and becomes NO_2^- adsorbed on the surface of the ZnO film resulting in the increase of the work-function of the ZnO. The response process is given by

$$NO_2 + e^- \rightarrow NO_2^- \quad (5)$$

Therefore, the I_D-V_{GS} curves and transient I_D behaviors of the *p*MOSFET gas sensor having a ZnO as a sensing layer moves positive direction and increases.

On the other hand, in H_2S ambience, the opposite response happens in the *p*MOSFET gas sensor. In air ambience, oxygen gases are adsorbed on the ZnO. Therefore, chemisorbed oxygen molecules are adsorbed on the surface of the ZnO in the form of O_2^- at 180 ^oC [59]. Absorbed O_2 molecules can be considered as a local acceptor. In H_2S ambience, H_2S molecules react with ionized O_2 adsorbed on the ZnO. The response process is given by

$$2H_2S + 3O_2^- \rightarrow 2H_2O + 2SO_2 + 3e^- \quad (6)$$

The adsorbed oxygen molecules decrease and the electrons are accumulated in the surface of the ZnO. Therefore, V_{th} of the *p*MOSFET gas sensor increases due

to the decrease of the work-function of the ZnO film, and the I_D decreases.

$$O_2 + e^- \rightarrow O_2^- \quad (7)$$

In order to recover, O_2 molecules in the air obtain electrons from the ZnO and adsorbed on the ZnO in the form of O_2^- as explained by (7). Due to the ionized O_2^- molecules, the work-function of the ZnO increases, which cause the increase of the I_D same as oxidizing gas reaction.

3.5 Resistor-type gas sensor

The resistor-type gas sensor is also fabricated using same fabrication process on the same wafer. The fabricated resistor-type gas sensor has a ZnO layer as a sensing material with area of 10^4 μm^2 (see Fig. 3.6 (a)). The *I-V* characteristic of the resistor-type gas sensor is measured by DC and PIV methods as shown in Fig. 3.7. The ZnO film deposited by ALD at 250 ^oC generally shows high *n*-type conductivity due to the zinc interstitial and oxygen vacancy working as donors [61]. Even though the work-function of the ZnO and CG is 4.3 eV and 5.1 eV, respectively, the carrier concentration of the ZnO is ~ 10^{20} cm^{-3}. Thus they form ohmic contact. From the measured results, *I-V* curves of the resistor-type gas sensor show they form ohmic contact. Fig. 3.8 shows transient current behaviors of the resistor-type gas sensor as a parameter of NO_2 concentration at 1 V., Since NO_2 is an oxidizing gas, an NO_2 gas molecule extracts an electron from the ZnO and becomes a NO_2^- adsorbed on the surface of ZnO. Therefore, the resistance of the ZnO layer increases, resulting in the decrease of current (*I*). At 0.5 ppm NO_2 ambience, the resistance was increased

from 1.73MΩ to 15.87 MΩ after NO_2 was injected.

Even though the resistor-type gas sensor shows a high response to NO_2 gas, the sensor needs a large area to decrease the resistance variation and to increase working current. The recovery rate is so slow that it takes ~1 hour to be fully recovered at 180 ^oC. Also, since the resistor-type gas sensor cannot control the electron concentration of the ZnO film by electrical method, there is a limitation to enhance the gas sensing property by the electrical method.

However, the FET-type gas sensor in this work is reliable and occupies a small area (~400 μm^2), and can be integrated with circuits on the same chip. More importantly, the proposed pulse pre-bias scheme can significantly improve the response and recovery property of the FET-type gas sensor.

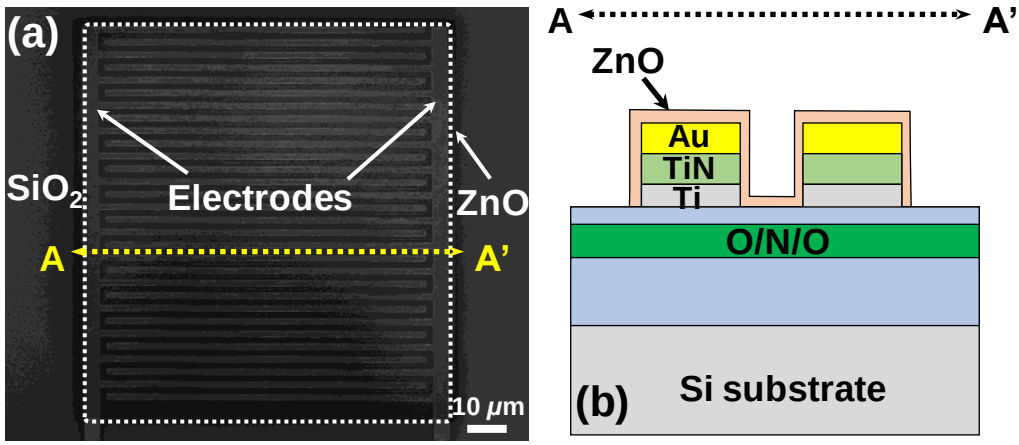

Fig. 3.6 (a) Top SEM image of the fabricated resistor-type gas sensor. (b) Schematic cross sectional view of the fabricated resistor-type gas sensor cut along a yellow dashed line A-A' in (a).

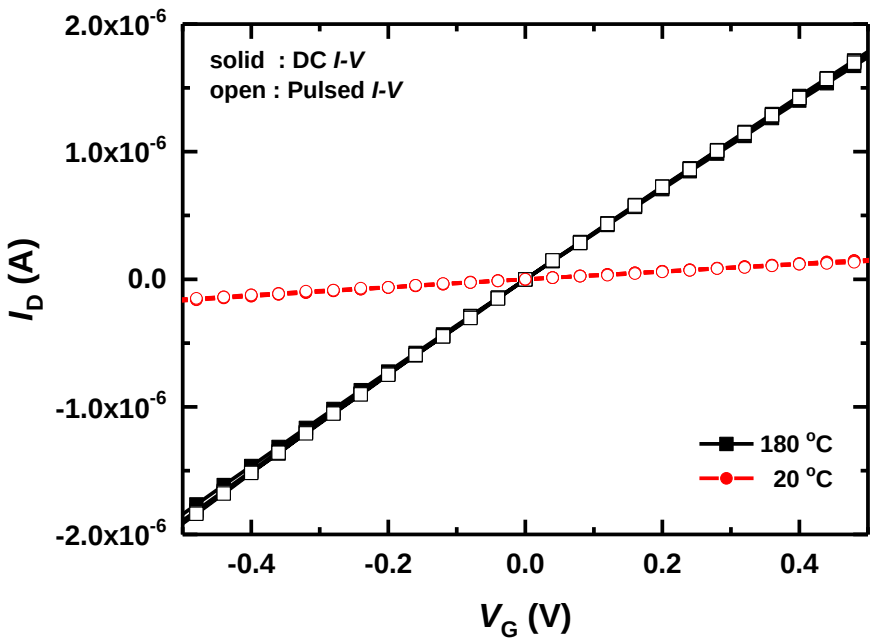

Fig. 3.7 *I-V* curves of the resistor-type gas sensor at RT (20 °C) and 180 °C.

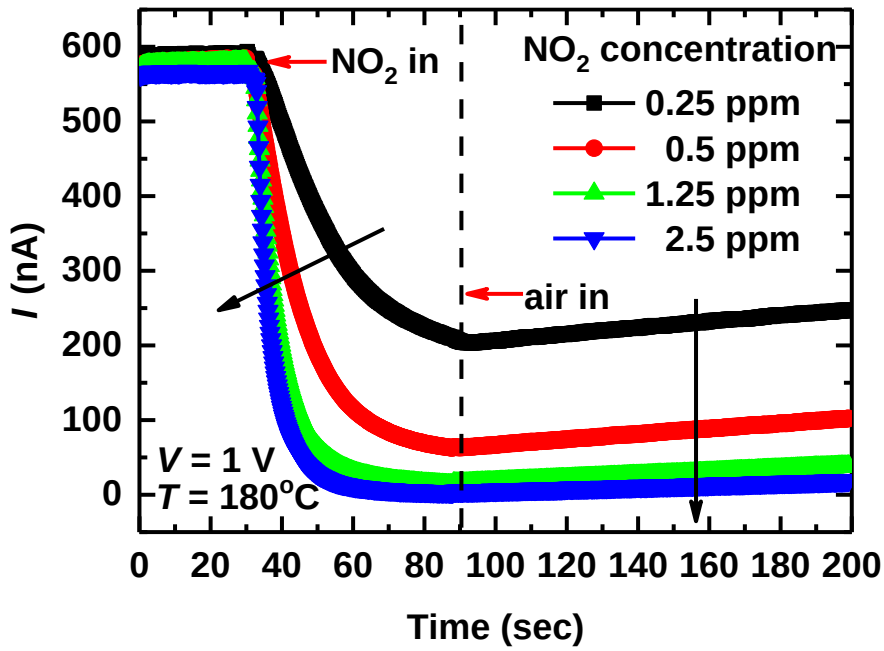

Fig. 3.8 Transient *I* behaviors of the resistor-type gas sensor as a parameter of NO_2 concentrations (0.25 ppm, 0.5 ppm, 1.25 ppm, and 2.5 ppm) at 180 °C.

Chapter 4

Proposed pre-bias pulse scheme and gas sensing characteristics

4.1 Motivation

Recently, to improve gas sensing characteristics, two kinds of techniques have been used, which are UV illumination and heating effect [38-41]. The electrons supplied by UV or heat enhance the adsorption and desorption of gas molecules. S. Zhang *et al.* reported the excess photo-generated electrons are increase the adsorption of the oxygen molecules [41]. In addition, the heating effect of the FET-type gas sensor having ZnO film as a sensing layer is reported in our previous research. Y. Hong *et al.* reported that transient I_D behaviors are measured at 20 ppm of NO_2 gas as a parameter of the temperature from 25 ^oC to 180 ^oC (Fig. 4.1) [28]. As the temperature increases, the response time and the recovery rate is significantly decreased. The increased kinetic energy of NO_2 molecules and excess electrons in ZnO film by high temperature increase the gas response and recovery property. However, these two methods need bulky

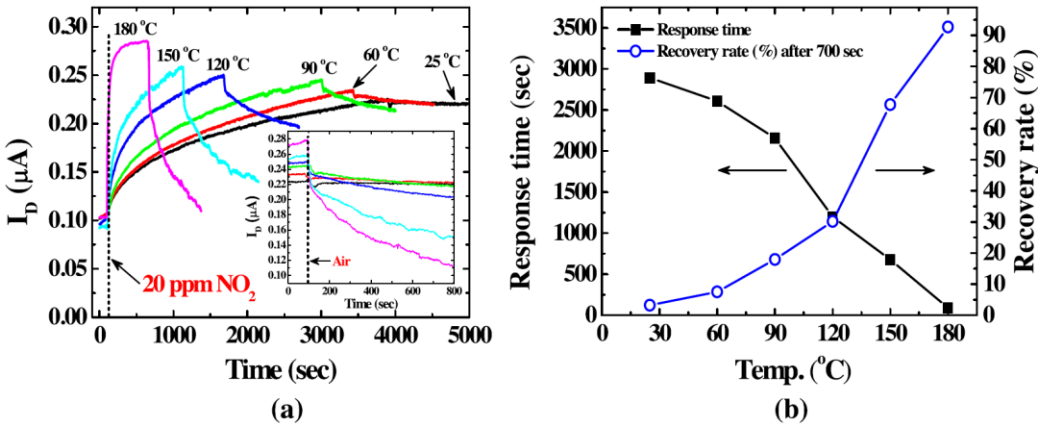

Fig. 4.1 Temperature effect on FET-type gas sensor in ref [28].

equipment such as external light source and heater, which is difficult to apply to the practical gas sensor. Although the FET-type sensors having a higher degree of freedom coming from four terminal features in enhancing the sensing performance, there has been no report on electrical control scheme.

In this paper, we investigate, for the first time, the pre-bias effect on response and recovery characteristics of Si FET-type gas sensor. A new pulse bias scheme for the pre-bias is devised to increase gas response and to reduce recovery time.

4.2 Proposed pulse pre-bias scheme

To improve the gas sensing characteristics of the FET-type gas sensor, the pre-bias pulse scheme is proposed. The schematic measurement system and pre-bias pulse scheme are illustrated in Fig. 4.2 and 4.3, respectively. The generated pulses from the WGFMU are simultaneously applied to the CG and drain electrode, and source is grounded. The V_{pre} and read bias (V_{rCG}) are alternatively applied to the CG with respective pulse widths of t_{pre} and t_{read}. The drain pulse (V_{rDS}) during read is synchronized with the V_{rCG}. In this research, the pre-bias from -3 V to 4 V is applied to the CG and V_{rCG} is fixed at 0 V which linear region of the FET-type sensor. The V_{rDS} is fixed at -0.1 V.

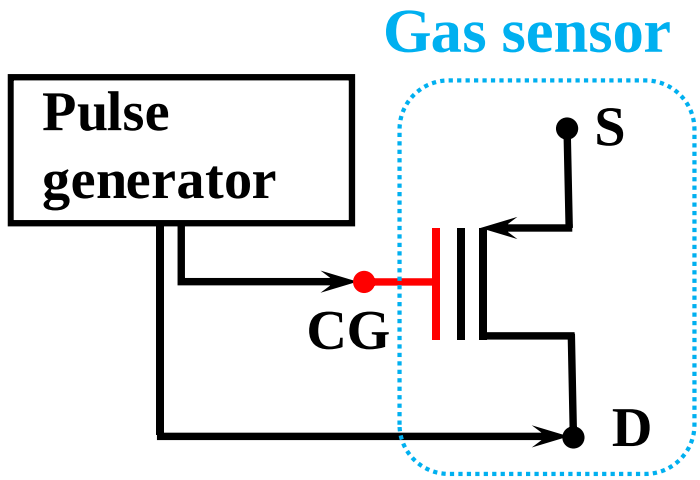

Fig. 4.2 Schematic image of the measurement system.

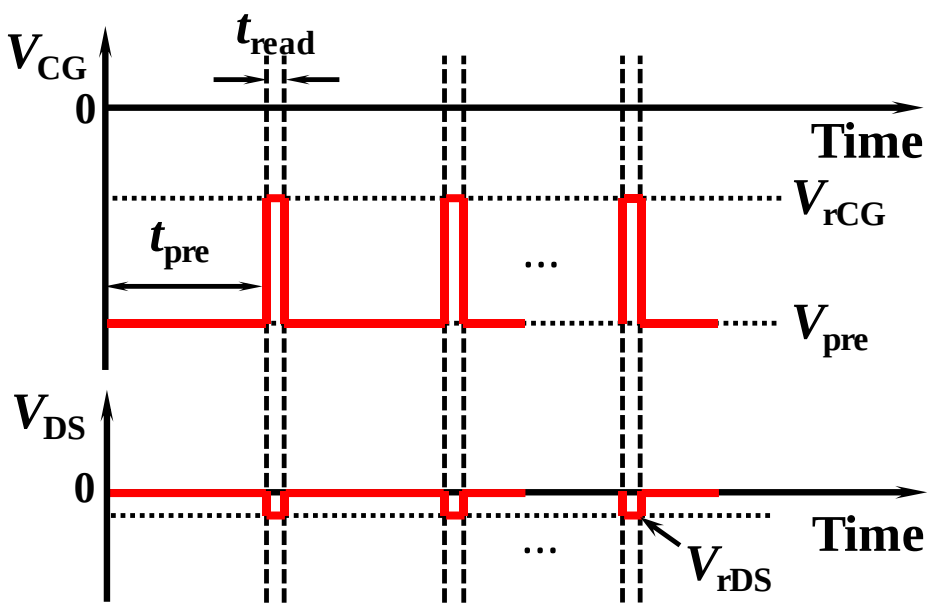

Fig. 4.3 Proposed pulse scheme for the pre-bias (V_{pre}) and read bias (V_{rCG}). The V_{pre} and V_{rCG} are applied to the CG alternatively with respective pulse widths of t_{pre} and t_{read}.

4.3 The Pre-bias effect

4.3.1 The Pre-bias effect on gas response

The transient I_D behaviors of the FET-type gas sensor are measured as a parameter of V_{pre} from -3 V to 2 V in 0.5 ppm NO_2 ambience at 180 ^oC (Fig. 4.4 (a)). The V_{rCG} and V_{rDS} are fixed at 0 V and -0.1V, respectively. The V_{pre} and V_{rCG} are applied to the CG alternatively with a t_{pre} of 0.1 s and a t_{read} of 5×10^{-5} s. As the V_{pre} decreases, the $|I_D|$ increases. It is quite interesting that the gas response significantly increases with negatively increasing the V_{pre}. Note the I_D is nearly constant when we apply the V_{pre} in air as represented by diamond symbols. As a reference, the transient I_D at a V_{pre} of -1 V shows no change in air ambience. This results shows that the pre-bias can increase the gas response to NO_2. Fig. 4.4 (b) shows gas response versus V_{pre} at a fixed NO_2 concentration of 0.5 ppm. Here, the response of the gas sensor to a target gas is defined as

$$\text{Response}(\%) = \frac{\left|I_{D,res}(t)\right| - \min\left|I_{D,air}\right|}{\min\left|I_{D,air}\right|} \times 100 \qquad (8)$$

Where $I_{D,res}(t)$ and $I_{D,\,air}$ stand for I_D at a t during response period and I_D before NO_2 is injected respectively. The response is calculated by using the equation (8) and the data in Fig. 4.4 (a). The response at a V_{pre} of -3 V is about 100 % which is ~2.5 times larger than that at a V_{pre} of 0 V.

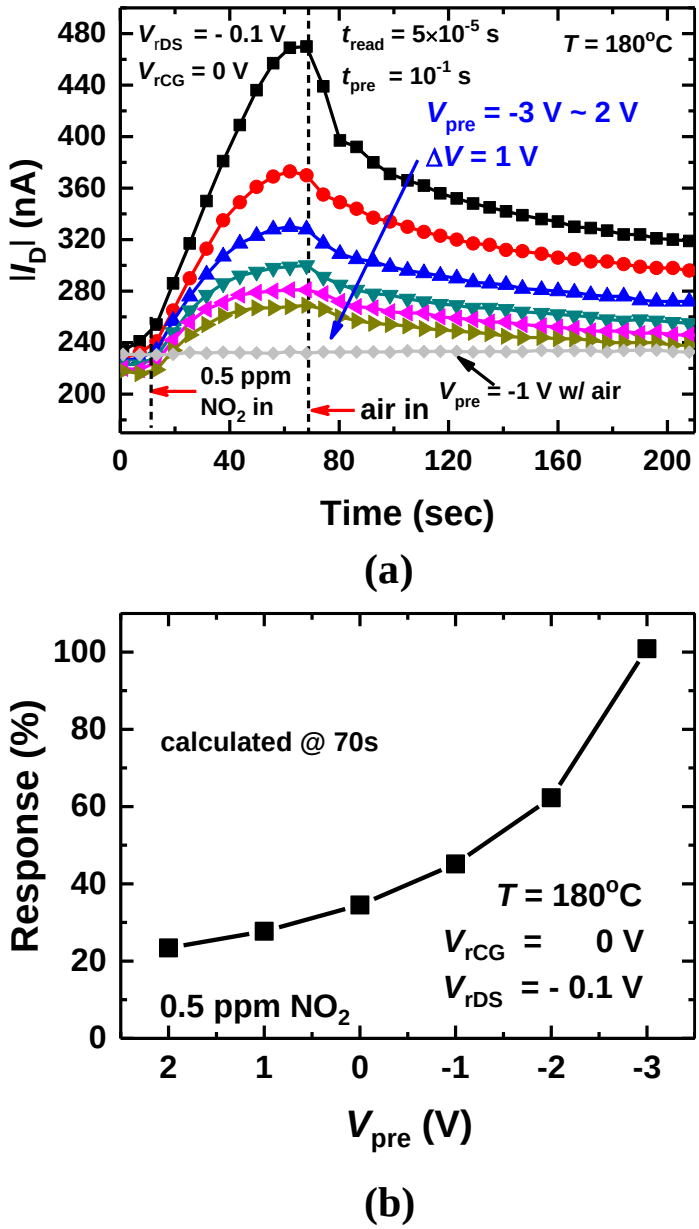

Fig. 4.4 (a) Transient I_D behaviors with different V_{pre}s in 0.5 ppm of NO_2. (b) Gas response versus V_{pre}, which is calculated by the equation (8) using measured I_D at t = 70 s in Fig. 4.4 (a).

4.3.2 Mechanism responsible for the pre-bias effect on gas response

The mechanisms of the pre-bias effect on the gas response and recovery characteristics of the Si FET-gas sensor is explained using energy band diagram. The work-function of the CG which is gold, the ZnO, and FG which is n^+ poly Si are 5.1 eV, 4.3 eV, and 4.1 eV. Since the ZnO film deposited by ALD generally shows high *n*-type conductivity due to the zinc interstitial and oxygen vacancy working as donors, fermi level of the ZnO is very close to the conduction band [62]. Thus, the CG and the ZnO form the ohmic contact. The energy band diagram at flat band condition is shown in Fig. 4.5. Since the gas reaction mainly occurs in ZnO, we have analyzed the pre-bias effect by focusing on the energy band diagram of the ZnO and both sides. The effect of the pre-bias is explained by dividing into gas response and gas recovery.

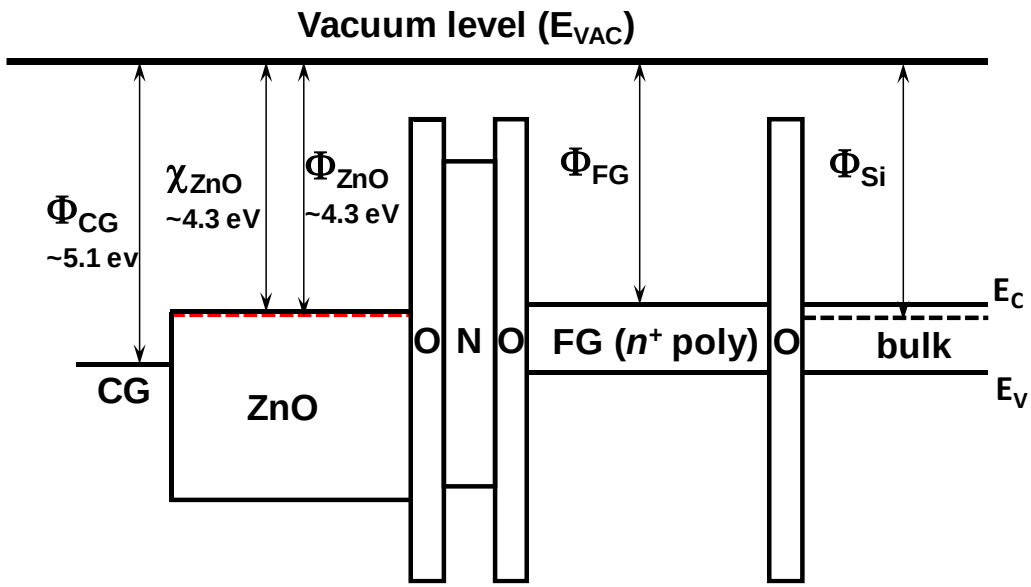

Fig. 4.5 Energy band diagram of the *p*MOSFET sensor at flat band condition.

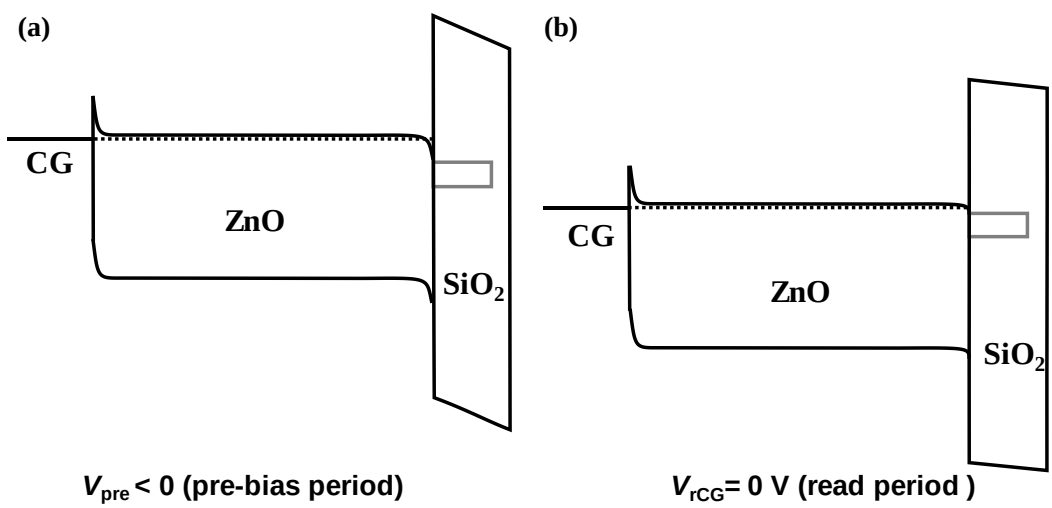

Fig. 4.6 Energy band diagram of the *p*MOSFET sensor in (a) pre-bias period by applying negative V_{pre} and (b) read period (V_{rCG} = 0 V) in air ambience.

To explain the pre-bias effect on gas response depending on the V_{pre}, the schematic energy band diagrams of the gas sensor with different V_{pre}s in air and NO_2 ambience are illustrated in the Fig. 4.6. At a given negative V_{pre}, as shown in Fig. 4.6 (a), the energy band diagram goes upward than read period as shown in Fig. 4.6 (b). When a negative V_{pre} is applied to the CG, electrons in ZnO are accumulated near the FG.

Schematic energy band diagrams of the FET-type gas sensor in the pre-bias period at different V_{pre}s and read period at a V_{rCG} of 0 V are illustrated in the Fig. 4.7. The solid and the dashed lines stand for the energy band diagrams before and after NO_2 exposure, respectively. Since the NO_2 is an oxidizing gas, an NO_2 gas molecule extracts an electron from the ZnO (chemisorption) and are adsorbed in the form of NO_2^- on the surface of ZnO. Thus, adsorbed NO_2 molecules can be represented as a local acceptor. The area of the rectangle at the interface represents the total amount of possible sites for the adsorption of NO_2 molecules and the filled area schematically refers to the amount of extracted electrons (Fig. 4.7 (a)).

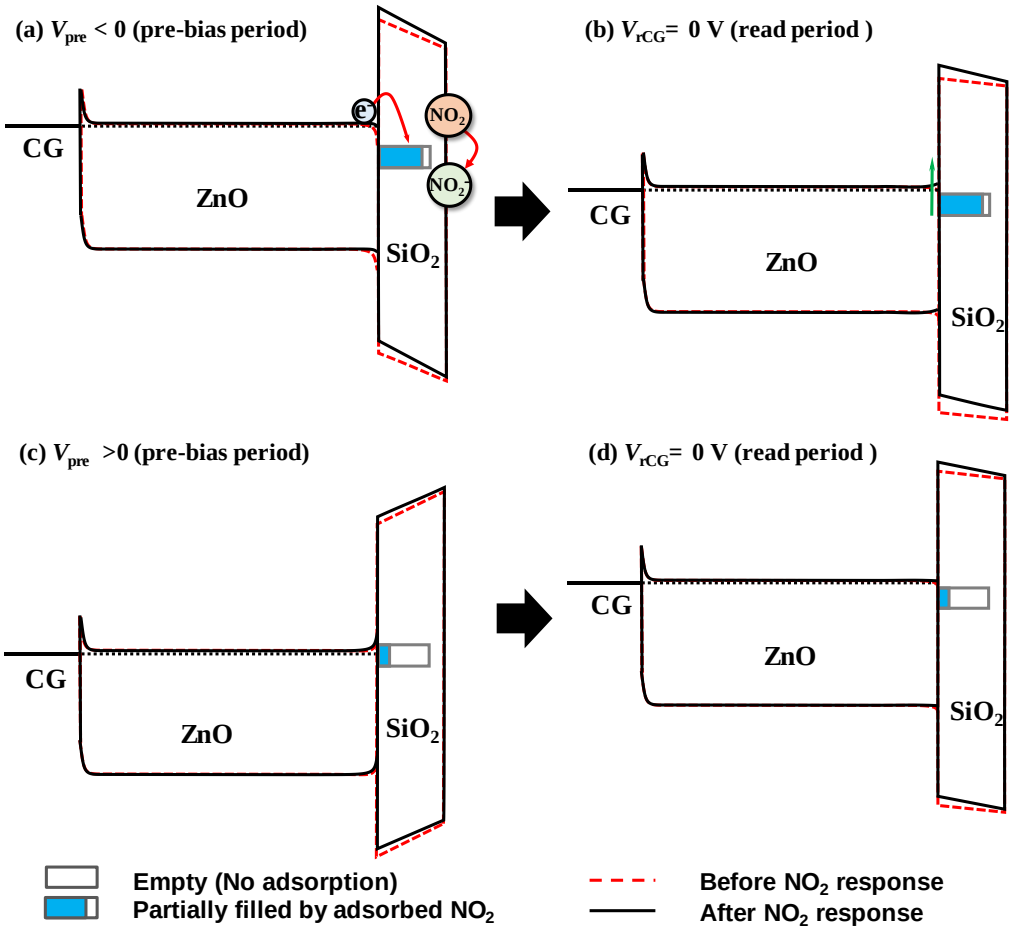

Fig. 4.7 Schematic energy band diagrams of the gas sensor in the pre-bias period at different V_{pre}s and read period at a V_{rCG} of 0 V. The solid and the dashed lines stand for the energy band diagrams before and after NO_2 exposure, respectively. The area of the rectangle at the interface represents the total amount of possible sites for the adsorption of NO_2 molecules and the filled area schematically refers to the amount of extracted electrons.

In the pre-bias period with a negative V_{pre}, when the gas sensor is exposed to the NO_2 ambience, NO_2 gases are ionized in the ZnO film except the depleted region near the CG (Au). Since the acceptor energy level of adsorbed NO_2 molecules is lower than the Fermi level of the ZnO film by negative V_{pre}, electrons are easily transferred to the adsorbed NO_2 molecules (Fig. 4.7 (a)). More NO_2 molecules can be ionized by the electrons accumulated near the interface between the ZnO and the ONO stack, which leads to the increased NO_2^- density. Density of the adsorbed NO_2^- is represented by the filled energy state as shown in the Fig. 4.7 (a). The electron concentration in ZnO decreases with increasing NO_2^- density, resulting in the increase of the work-function of the ZnO. In read period (Fig. 4.7 (b)), as the work-function of the ZnO increases by the adsorbed NO_2^-, the V_{th} of the gas sensor decreases, which results in the increase of the transient $|I_D|$. As the V_{pre} increases negatively, the Fermi level of the ZnO becomes higher than the acceptor level of adsorbed NO_2. Thus, when a negative V_{pre} is applied to the CG, larger number of NO_2 are adsorbed on the ZnO, which cause the increase of the $|I_D|$ as shown in Fig. 4.4 (a).

In the pre-bias period with positive V_{pre}, since the ZnO film near the interface is depleted by the positive V_{pre}, NO2 molecules are hard to response at the interface between ZnO and ONO stack. Instead, NO_2 molecules are ionized in the ZnO film except both edge regions. Thus, small amount of NO_2 molecules react, which cause the energy band to rise slightly as depicted in the Fig. 4.7 (c). In read period (Fig. 4.7 (d)), as the V_{pre} increases positively, the Fermi level of the ZnO becomes lower than the acceptor level of adsorbed NO_2. Thus, when a positive V_{pre} is applied to the CG, NO_2 molecules are slightly adsorbed on the ZnO, so that the $|I_D|$ is increased little as shown in Fig. 4.4 (a). Thus, an improved gas response can be obtained by applying a negative V_{pre} to the oxidizing gas such as NO_2.

4.3.3 The Pre-bias effect on gas recovery

To confirm the pre-bias effect on the recovery characteristic, the transient I_D is measured at 180 °C with different V_{pre}s during the recovery period (t > 73 s in Fig. 4.8 (a)). The V_{pre} is fixed at -1 V in the response period (10 < t < 73 s), and is changed from -1 V to 4 V in the recovery period. As the V_{pre} increases, the I_D is quickly recovered to the base level, which is 230 nA. At a V_{pre} of 4 V, I_D is fully recovered within a minute. Here, the recovery of the gas sensor to a target gas is defined as

$$\text{Recovery}(\%) = \frac{\max\left|I_{D,res}\right| - \left|I_{D,rec}(t)\right|}{\max\left|I_{D,res}\right| - \min\left|I_D\right|} \times 100 \quad (9)$$

where $I_{D,rec}$ is the I_D in the recovery period and $I_{D,res}$ is the I_D in the response period. The recovery is calculated by using the equation (9) and the data in Fig. 4.8 (a). At a V_{pre} of 4 V, full recovery time is 60 s which is 9 times faster than that at a V_{pre} of 0 V (typical). The recovery characteristics sampled at 73 s (square) and 143 s (circle) with the V_{pre} are shown in Fig. 4.8 (b). The slopes are nearly same regardless of V_{pre} at different sampling time. This result shows that there is no pre-bias effect during the recovery period. This phenomenon is explained in details in the Ch. 4.3.4.

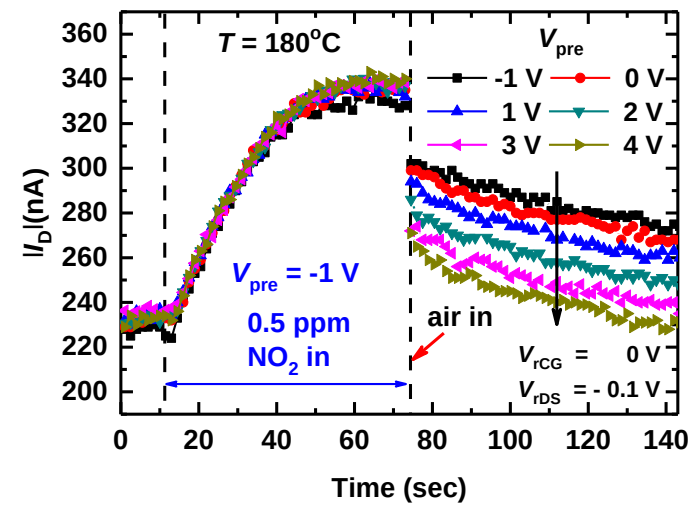

(a)

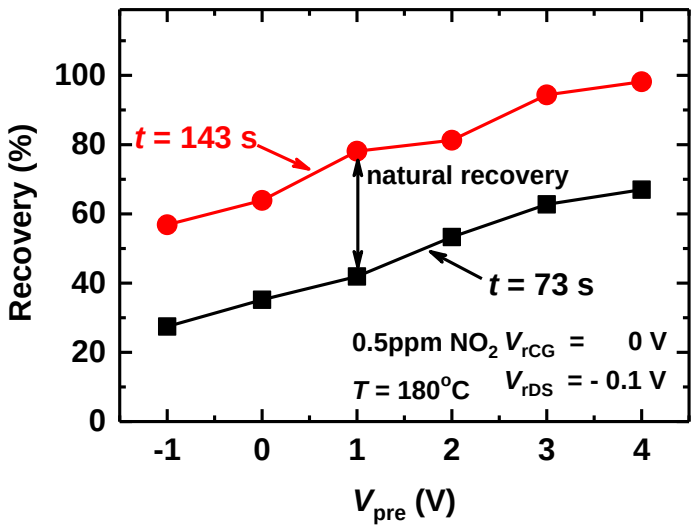

(b)

Fig. 4.8 (a) Transient I_D behaviors with different V_{pre}s (-1 V ~ 4 V) during the recovery period (t > 76 s). In the response period (10 < t < 73 s), the V_{pre} is fixed at -1 V. (b) Recovery versus V_{pre} as a parameter of sampling time in the recovery period.

4.3.4 Mechanism responsible for the pre-bias effect on gas recovery

To explain the mechanism of desorption in the recovery period with the V_{pre}, schematic energy band diagram is depicted in Fig. 4.9 (b). When a negative V_{pre} is applied to the CG in the response period, the band structure of ZnO film is represented by the dashed line. After the gas sensor with a positive V_{pre} is exposed to air in the recovery period, the band diagram near the interface between the ZnO and the O/N/O stack changes. Since the acceptor energy level of adsorbed NO_2 molecules is higher than the Fermi level of the ZnO film by positive V_{pre}, electrons from adsorbed NO_2^- molecules are easily transferred to the ZnO. The adsorbed NO_2^- molecules near the interface are quickly desorbed by transferring electrons to the ZnO at the positive V_{pre} as represented by the process ① in Fig. 4.9 (b). Therefore, the I_D is significantly decreased at the beginning of the recovery period as the V_{pre} increase (Fig. 4.8 (a)). The NO_2^- molecules adsorbed in the ZnO film except the interface between ZnO and ONO stack are subsequently desorbed during the whole recovery period as represented by the process ②. Thus, the slopes are nearly same regardless of V_{pre} at different sampling time. Due to the decrease of work-function of the ZnO, the I_D of the sensor returns to that in air ambience. From the result, the pre-bias effect on the recovery characteristics mostly occurs at the beginning of the recovery period.

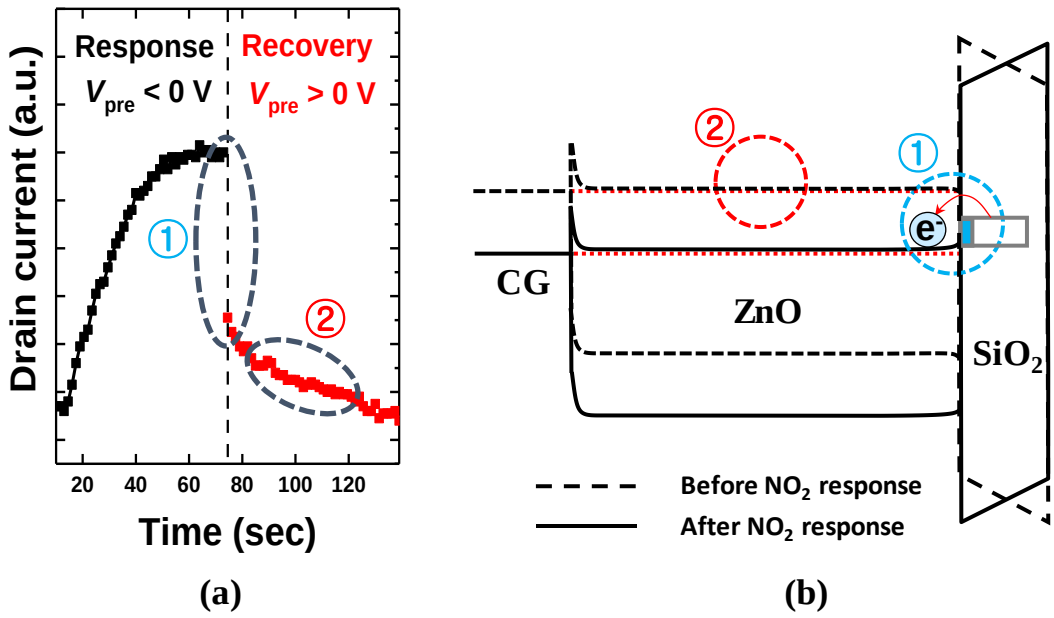

Fig. 4.9 (a) Response with a negative V_{pre} and recovery with a positive V_{pre}. (b) Schematic energy band diagram to explain desorption of NO_2 with a positive V_{pre} during recovery period. The sequence of the desorption is depicted by ① and ②.

4.4 Gas response to different concentration of NO_2 gas

Fig. 4.10 shows the transient I_D behaviors of the sensor as a parameter of NO_2 concentration at V_{pre} = -2 V. As the NO_2 concentration increases, the transient I_D increases. Fig. 4.11 shows gas responses versus concentration of NO_2 as a parameter of V_{pre} from -2 V to 2 V. In general, the gas responses are saturated at high concentration of the gas. As shown in the Fig. 4.11, unlike gas responses obtained by V_{pre}s of 0, 1, and 2 V are saturated at 2.5 ppm NO_2 ambience, gas response obtained by negative V_{pre} increases as the NO_2 concentration increases. Thus, by negatively increasing the V_{pre}, we can extend linear response region with the concentration. Also, by the negative V_{pre}, we can significantly improve the gas response. In the inset, the response at a V_{pre} of -2 V is ~1.5 times larger than that at a V_{pre} of 0 V in 250 ppb NO_2 ambience.

To check the sensing performance at extremely low concentration of NO_2, the transient I_D behaviors (Fig. 4.12 (a)) are firstly measured for 50 s and then I_D-V_{CG} curves (Fig. 4.13 (a)) are measured as a function of NO_2 concentration from 25 ppb to 1000 ppb. Fig. 4. 12 (a) and (b) shows transient I_D behaviors and

response of the FET-type gas sensor as a function of NO_2 concentration on a logarithmic scale at V_{pre} of -2 V. By applying V_{pre} of -2 V, 25 ppb of NO_2 is successfully detected and the response is 5.8 %. Fig. 4.13 (a) shows the I_D-V_{CG} curves as a parameter of NO_2 concentration. As mentioned in the sensing mechanism Ch. 3.4, the work-function and capacitance of the ZnO can be changed by the adsorbed NO_2^- molecules. As the NO_2 concentration increases, the I_D-V_{CG} shifts in the positive direction From the results, at 25 ppb to 500 ppb of NO_2, the work-function increase of the ZnO is dominant by adsorbed NO_2^- molecules, which cause the V_{th} shift. Fig. 4.13 (b) shows V_{th} shift versus NO_2 concentration. The *V*th shifts from 35 mV to 182 mV as the NO_2 concentration increase from 25 ppb to 500 ppb. However, at above 500 ppb of NO_2, the slopes of I_D-V_{CG} curves decrease. As the NO_2 concentration increases, the depletion in the ZnO film increases by adsorbed NO_2^- molecules. The capacitance of the ZnO decreases resulting in the decrease of the coupling ratio. Therefore, at above 500 ppb of NO_2, the slopes of the I_D-V_{CG} curves decrease.

Thus, by applying the negative V_{pre} to the CG, it is possible to detect the

extremely low concentration of NO_2 and to extend the detection range by increasing the saturated concentration.

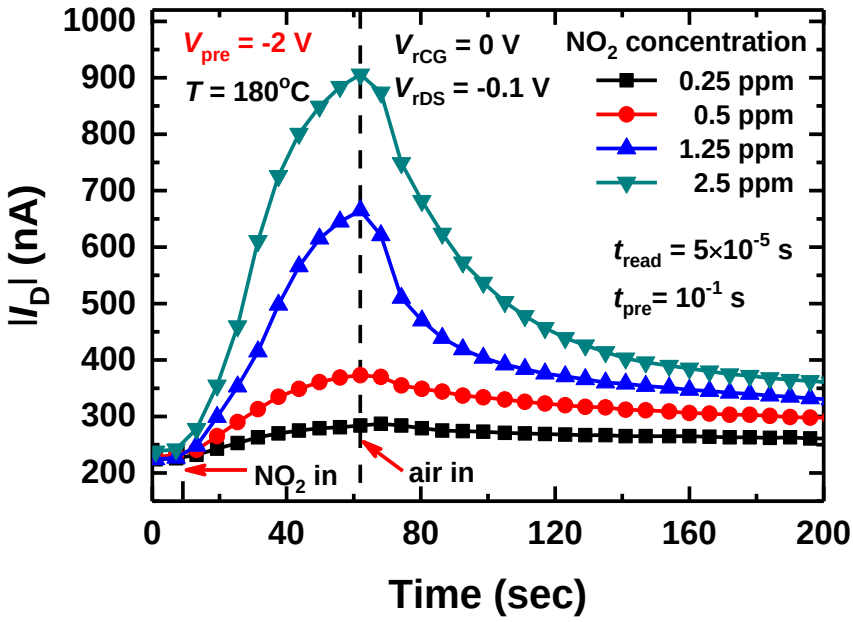

Fig. 4.10 Transient I_D behaviors as a parameter of gas concentration at V_{pre} = -2 V.

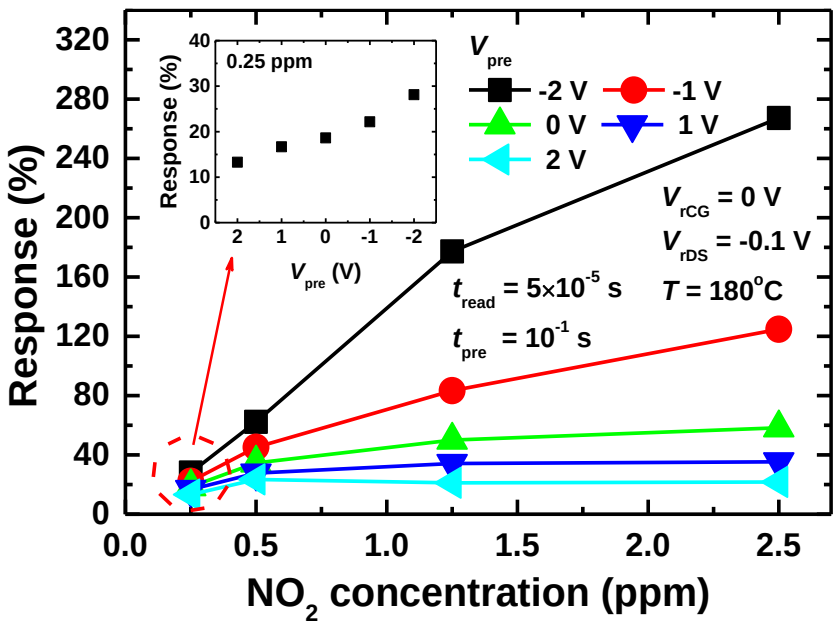

Fig. 4.11 Gas response versus gas concentration as a parameter of V_{pre} (from -2 V to 2 V). The insert represents gas response versus V_{pre} at 0.25 ppm.

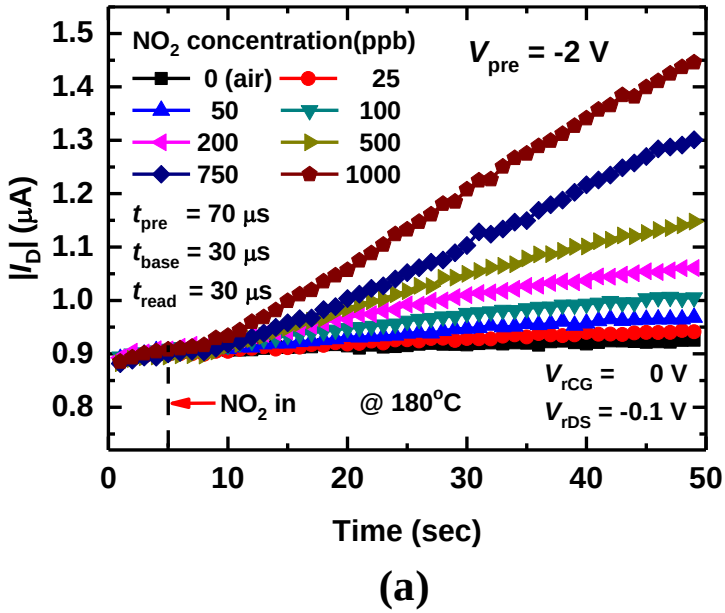

(a)

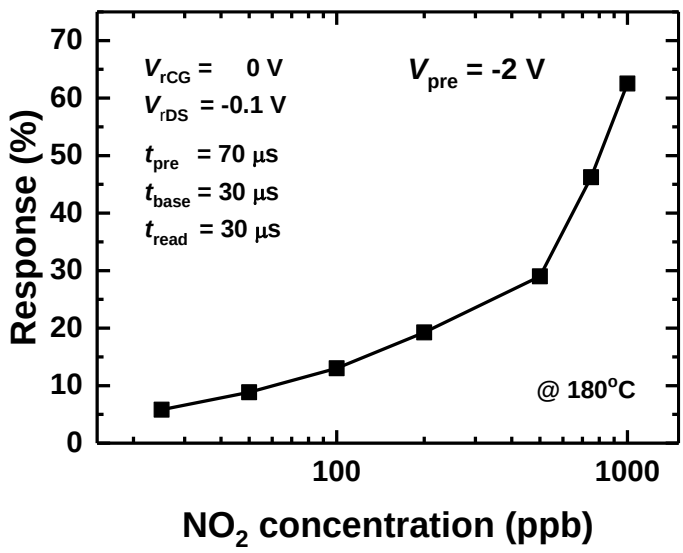

(b)

Fig. 4.12 (a) Transient I_D behaviors and (b) response of the FET-type gas sensor as a function of NO_2 concentration on a logarithmic scale at -2 V of V_{pre}. The FET-type gas sensor can detect 25 ppb of NO_2.

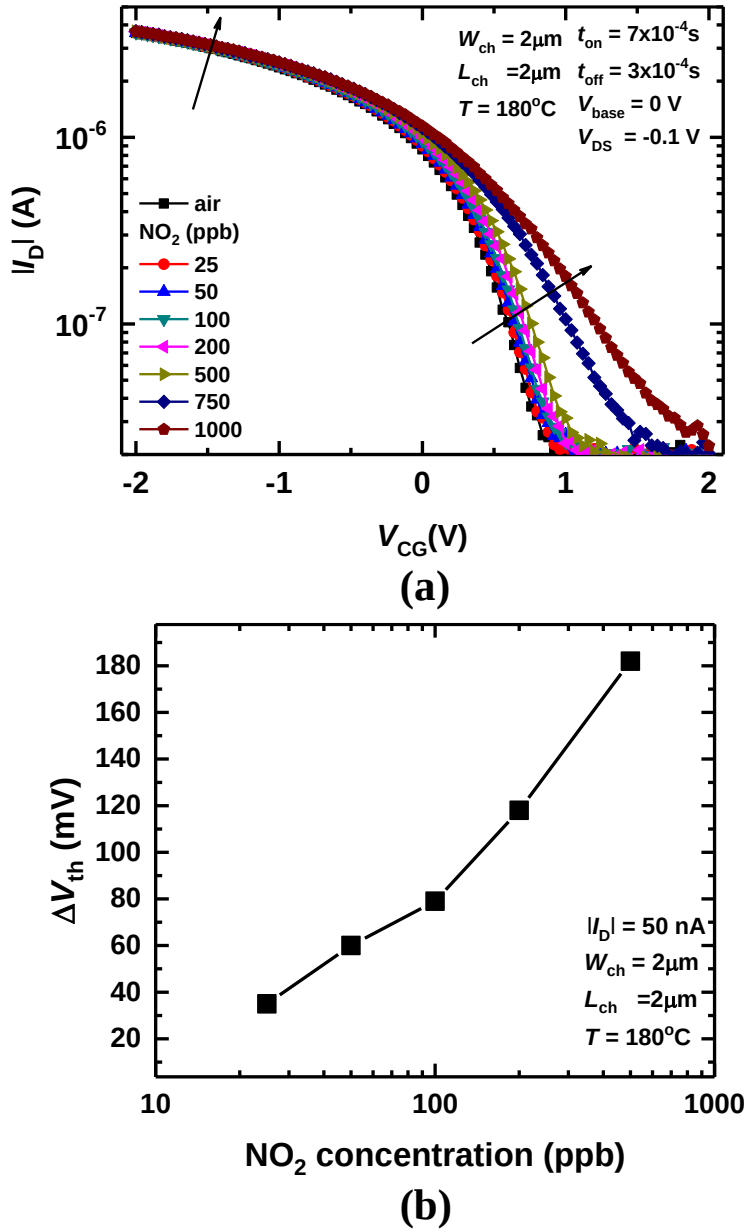

Fig. 4.13 (a) I_D-V_{CG} curves as a parameter of the NO_2 concentration at 180 °C. (b) V_{th} shift versus NO_2 concentration from 25 ppb to 500 ppb.

4.5 Optimal pulse pre-bias scheme

The proposed pulse pre-bias scheme is very efficient in improving the gas sensing performance of the Si FET-type gas sensor. By applying the negative V_{pre}, the gas response to NO_2 significantly increase. In addition, the recovery time to NO_2 target gas is considerably reduced by applying positive V_{pre}. Thus, we proposed optical pulse scheme for detecting oxidizing gas such as NO_2, NO, SO_2, CO_2, and etc. as shown in Fig. 4.14. In the response period, since the oxidizing gas acts as a local acceptor, a negative V_{pre} is applied to the CG to increase the Fermi level of the sensing material than acceptor level of the target gas. The electrons from the sensing material are transferred to the gas molecules, which cause the ionization of the target gas. The magnitude of negative V_{pre} applied to increase the gas response can be differed from the work function of the sensing material and acceptor level of the target gas.

In the recovery period, to desorb the adsorbed oxidizing gas molecules, a positive V_{pre} can be enhance the recovery time by lowering the Fermi level of the sensing material than the acceptor level of the adsorbed gas molecules. Thus,

electrons are easily transferred to the sensing material resulting in the desorption of the gas molecules.

By applying the optimal pulse pre-bias scheme, the repeated gas responses are measured in 0.5 ppm NO_2 at 180 ^{o}C (Fig. 4.15). The V_{pre}s for the response and recovery periods are -1 V and 2 V, respectively. V_{rCG} and V_{rDS} pulses are fixed at 0 V and -0.1 V, respectively. In comparison with DC response, the response is 7 time larger than that of DC and the recovery time decreases about 1/16. This result indicates that the gas sensing characteristic is significantly enhanced by applying negative V_{pre} in the response period and positive V_{pre} in the recovery period.

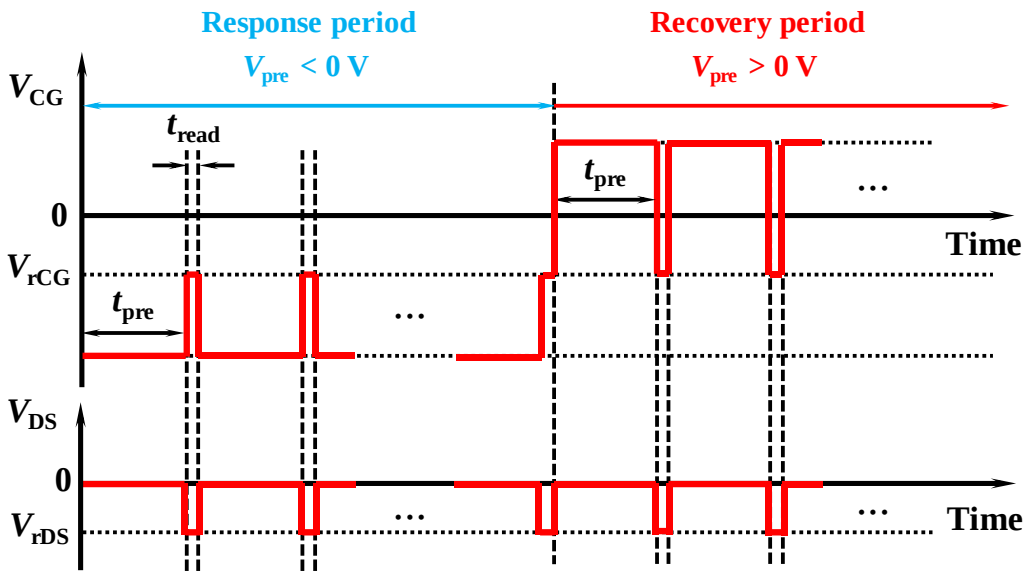

Fig. 4.14 Optimal pulse pre-bias scheme for oxidizing gas.

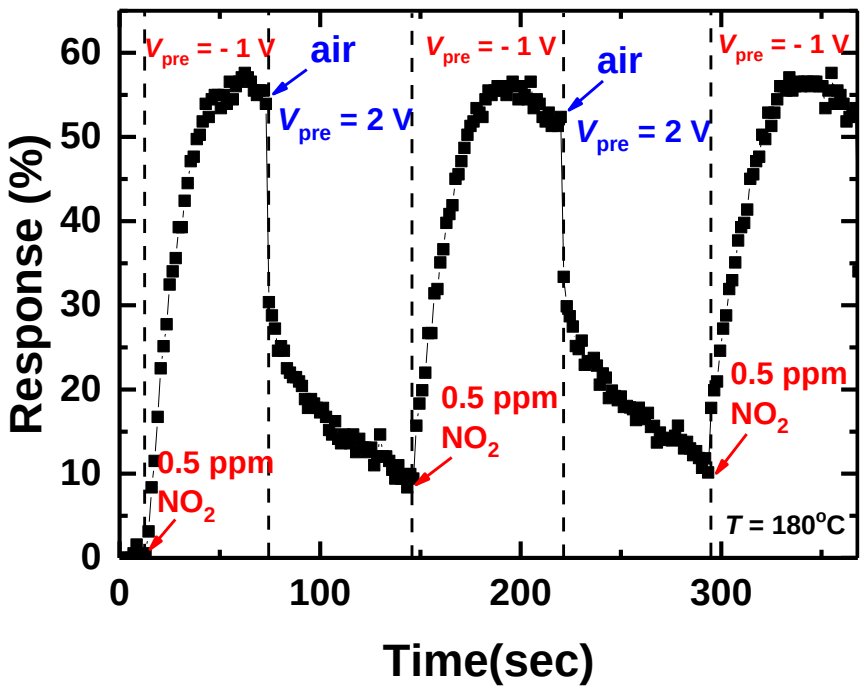

Fig. 4.15 Repeated 0.5 ppm NO_2 gas responses measured at 180 °C. The V_{pre}s for the response and recovery periods are -1 V and 2 V, respectively. V_{rCG} and V_{rDS} pulses are fixed at 0 V and -0.1 V, respectively.

4.6 The advantage of the pre-bias effect

Since the drain bias in the pre-bias period is fixed by 0 V, there is no current flow in the pre-bias period. Therefore, the power consumption of the FET-type gas sensor can be reduced by the pulse pre-bias scheme. Also, conventional method to reduce the recovery time is to increase the temperature of the sensor, which clearly increase the power consumption of the heater. However, by using pulse pre-bias pulse scheme, the recovery speed is significantly increased by applying the positive V_{pre}. Fig. 4. 16 shows the comparison of the recovery characteristics between pulse pre-bias scheme and DC measurement. Dashed lines represents gas responses measured at different temperature from 160 ^{o}C to 220 ^{o}C by applying DC 0 V. Here, V_{CG}-V_{th} is fixed at 0.4 V to avoid the V_{th} change with temperature. As the temperature increases, the response rate slightly increases the recovery speed significantly increases, whereas the response is degraded [28]. Gas responses represented by solid line and symbol are measured data with different V_{pre} from 1 V to 4 V in the recovery period at 180 ^{o}C. In the response period, V_{pre} of -1V is applied to the CG. The recovery characteristics applied by V_{pre} of 3V is nearly same as that of a DC result at 220 ^{o}C. Thus, by applying pre-bias scheme, response

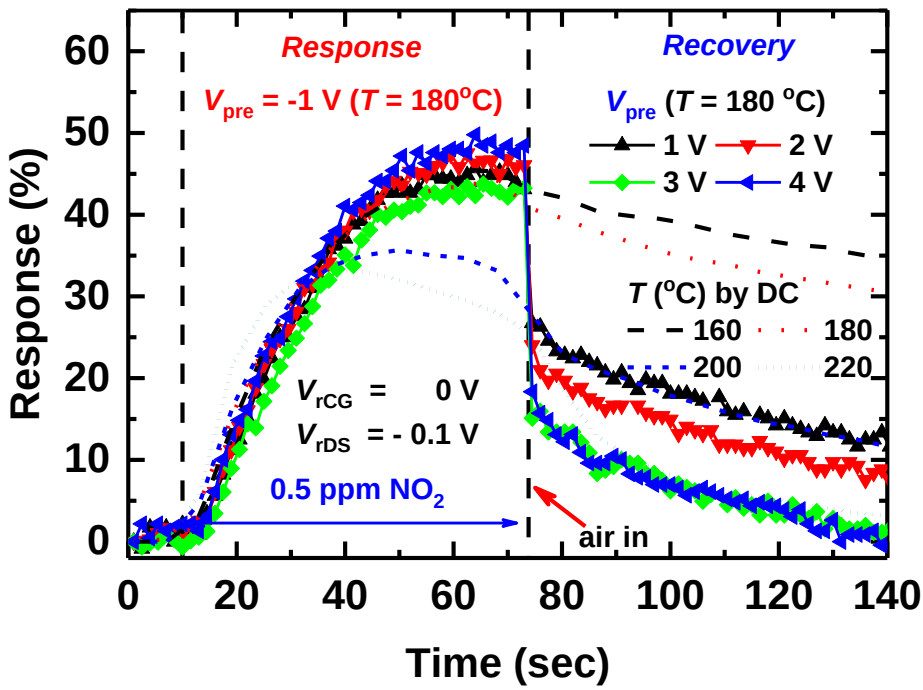

Fig. 4.16 Comparison of the recovery characteristics with DC measurement at different temperature from 160 °C to 220 °C by applying V_{CG} of 0 V. Responses represented by solid line and symbol are measured data with different V_{pre} from 1 V to 4 V in the recovery period at 180 °C. In the response period, V_{pre} of -1V is applied to the CG.

4.7 The pre-bias effect on reducing gas in recovery period

On contrary to oxidizing gas, when the reducing gas such as H_2S, CO, NH_3, H_2, and etc. are adsorbed on the sensing material, electrons are transferred to the sensing material. Detailed sensing mechanism of the reducing gas is explained by (6) in the Ch. 3.4. The reaction of reducing gas is explained by the adsorption and desorption of O_2 molecules. In the recovery period, O_2 molecules in the air obtain electrons from the sensing material and become ionized O_2 molecules adsorbed on the sensing material, which is the recovery from the reducing gas response. Thus, fast recovery can be realized by applying a negative V_{pre}. Since more electrons are accumulated at the interface between the sensing material and SiO_2 by the negative V_{pre}, the adsorption of O_2 molecules can be accelerated.

Fig. 4.17 shows transient I_D behaviors with different V_{pre}s in 16 ppm of H_2S at 180 ^oC. As the V_{pre} is changed from -4 V to 2 V, the gas response and recovery is nearly same regardless of V_{pre}. Electrons from desorbed O_2 molecules in the response period cannot changed the work-function of the ZnO because the carrier concentration of the ZnO is about 10^{20} cm^{-3}. This means that the Fermi level doesn't changed by electrons from O_2 molecules. Thus, transient I_D behaviors changes little. To prove the pre-bias effect on reducing gas in recovery period, further study is needed by changing the sensing material having lower concentration.

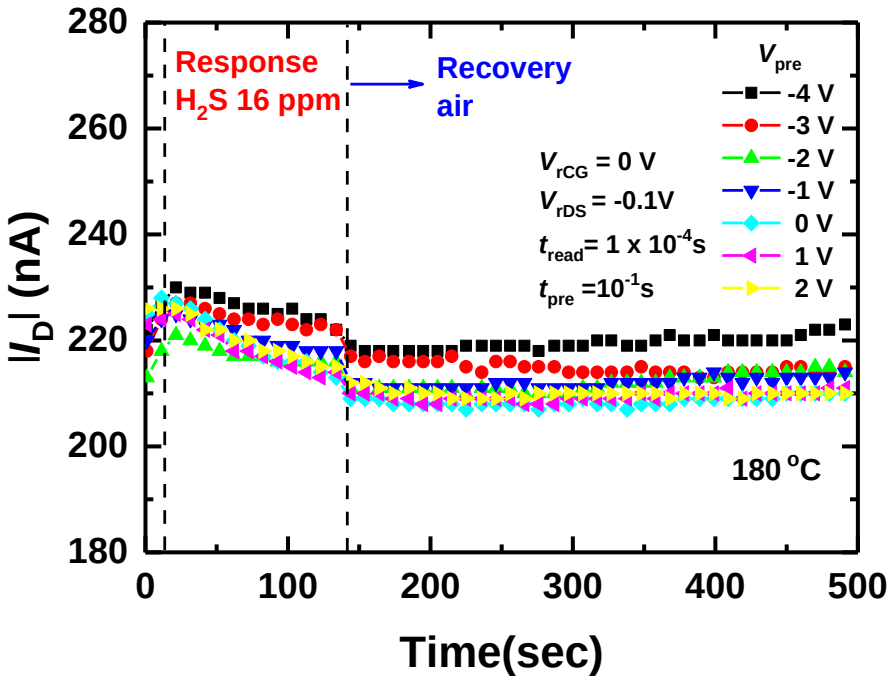

Fig. 4.17 Transient I_D behaviors with different V_{pre}s in 16 ppm of H_2S at 180 °C

Chapter 5

Conclusions

In this dissertation, a new pulse pre-bias scheme has been proposed to enhance significantly the sensing performance of Si FET-type gas sensor.

Firstly, the Si FET-type gas sensors having a FG in horizontal direction and Si MOSFETs which is composed by the peripheral circuits are fabricated at the same time. Since the *p*MOSFET shows lower 1/f noise than *n*MOSFET, the *p*MOSFET sensors and *p*MOSFETs are mainly fabricated. The simulation study for channel implantation is carried by TCAD device simulator. The ZnO film deposited by ALD is used for sensing material.

The electrical characteristics of the fabricated FET-type gas sensor are measured. By applying the PIV method, the transfer and output characteristics of the fabricated FET-type gas sensor are measured. To better understand the reaction between the FET-type gas sensor and gas molecules, the electrical modeling by resistor and capacitor is carried out. In addition, the nonvolatile memory function of the FET-type gas sensor is successfully confirmed by

program & erase and retention characteristics.

Finally, the pre-bias pulse scheme is proposed for improving the gas response and recovery characteristics. With respect to NO_2 which is representative oxidizing gas, the scheme was verified to be very efficient in improving the gas response and the reduction of the recovery time to NO_2 target gas. The response to NO_2 is significantly increased by applying the negative pre-bias in the response period and the recovery time is drastically reduced by positive pre-bias in the recovery period. The mechanism responsible for the pre-bias effect was analyzed by energy band diagram. It is expected that the pre-biasing scheme will be very practical in the commercialization of FET-type gas sensor.

Appendix A. Considerations for the pulse pre-bias scheme

A.1 Effect of the pulse width (t_{pre}) of pre-bias

The effect of the t_{pre} is investigated in the gas response period. The t_{pre} varies from 500 μs to 0.1 s and t_{read} is fixed at 50 μs. A V_{pre} of -1 V is applied to the CG. The transient I_D behaviors of the t_{pre} are shown in Fig. A.1. Regardless of the t_{pre}, the gas response at a V_{pre} of -1 V are nearly same. From the results, t_{pre} of 500 μs is enough to have the pre-bias effect in response period.

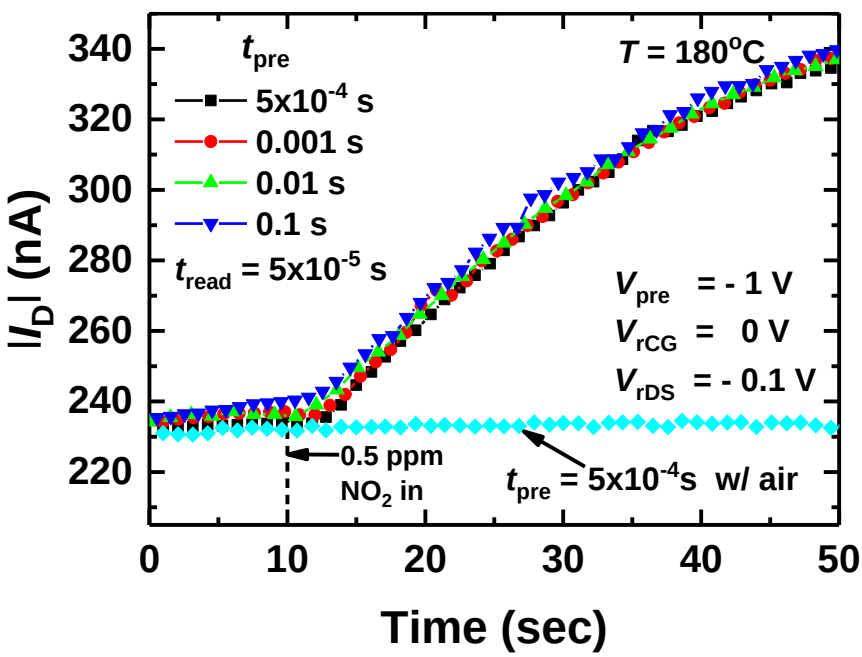

Fig. A.1 Transient I_D behaviors as a parameter of t_{pre}s from 500 μs to 0.1s in response period.

A.2 Effect of the carrier gas.

To adjust the concentration of NO_2, carrier gas and target gas of NO_2 are mixed while maintaining the total amount of gas. Since we use air as a carrier gas, the effect of oxygen in air which is also known as an oxidizing gas should be confirmed at a negative V_{pre}. Two kinds of carrier gas which is air and N_2 are investigated. From the result shown in Fig. A.2, the effect of oxygen is negligible. Therefore, the response is coming from NO_2 gas reaction at a negative V_{pre}.

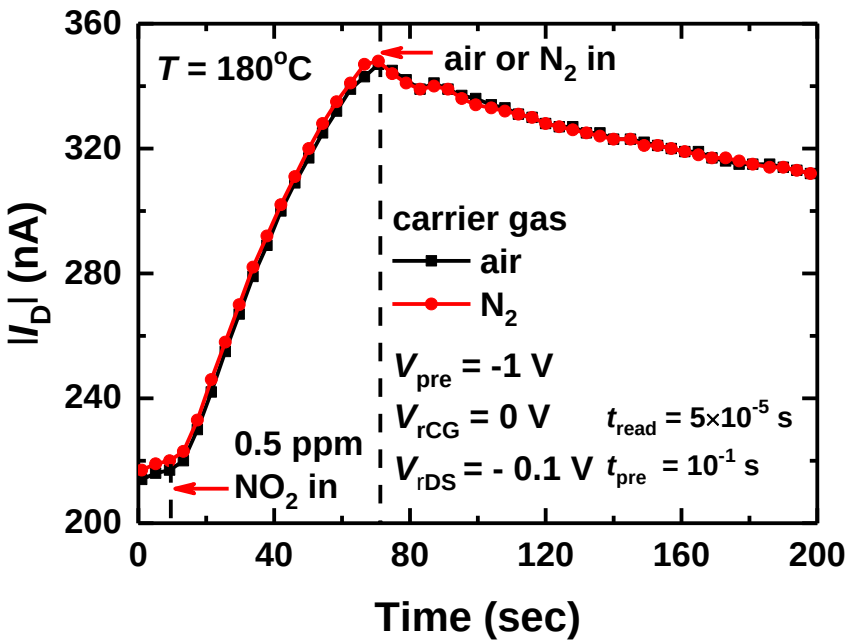

Fig. A.2 The effect of the carrier gas. The effect of oxygen gas is negligible.

Appendix B. Capacitance change FET-type gas sensor

As mentioned above in the Chapter 3.4, the sensing mechanism of the FET-type gas sensor, in this research, is based on the change of the work-function and the capacitance change of the sensing material. When the gas molecules are adsorbed on the sensing material, the change of the work-function and the capacitance of the sensing material simultaneously occur. Therefore, to analyze the sensing mechanism accurately, we propose a new FET-type sensor structures with capacitance change by using the same fabrication process. We denote the capacitance change FET-type gas sensor as the CFET gas sensor.

Fig. B.1 (a) shows the mask layout of the CFET gas sensor. By forming the contact hole to the FG, floating electrode attached to the FG is formed, when the CG electrode is formed. And then, the sensing material is formed on the CG electrode and floating electrode. Fig. B.1 (b) shows the schematic cross-sectional view of the CFET gas sensor along the dotted line A-A' in (a). Since the CG and FG are connected through the sensing material, the gate work-function of the CFET gas sensor is same as the work-function of the FG which is normally used by n^+ poly Si. Thus, when the gas molecules are adsorbed on the sensing material, the capacitance of the sensing material is changed. The capacitance change of the sensing material lead to the change of γ, resulting in the I_D change.

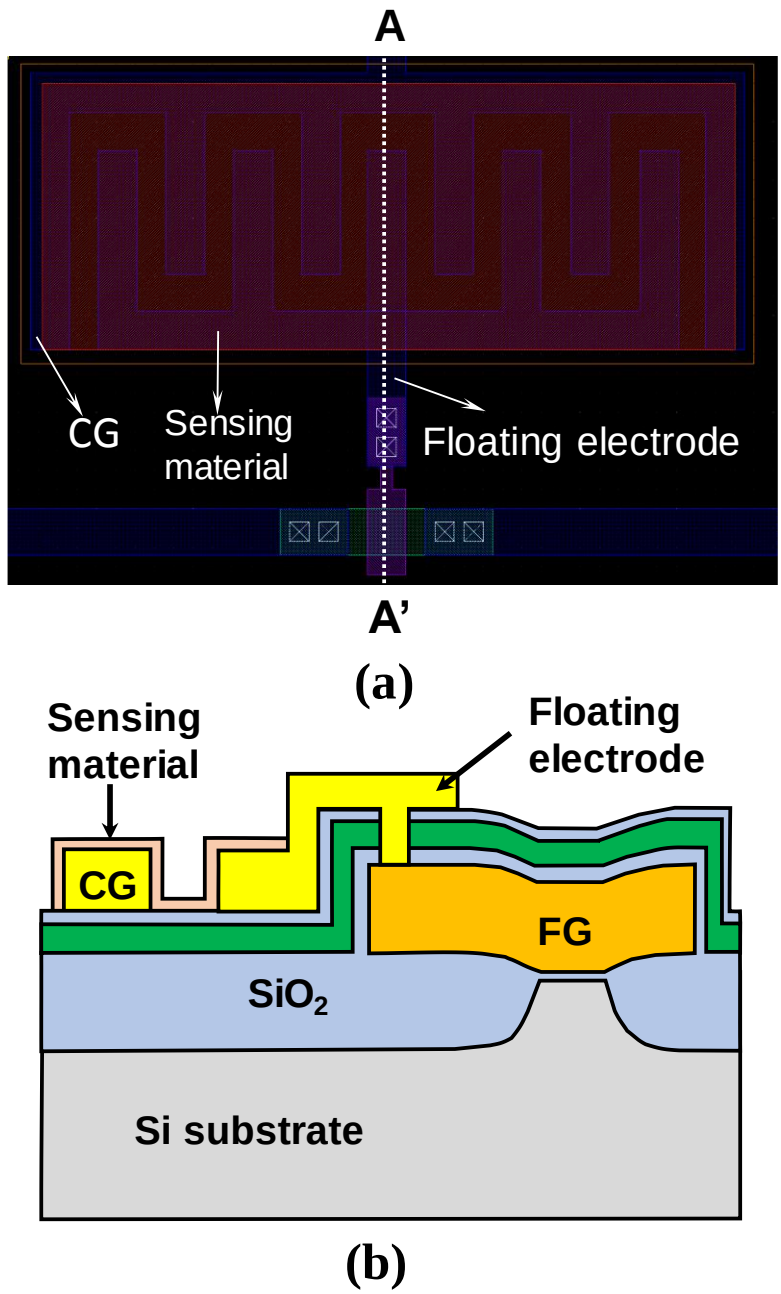

Fig. B.1. (a) Mask layout of the CFET gas sensor. (b) Schematic cross-sectional view of the CFET gas sensor along the dotted line in (a).

Bibliography

[1] P.M. Ramos, J.M. D. Pereira, H.M.G. Ramos, A. L. Ribeiro "A Four-terminal water-quality-monitoring conductivity sensor", *IEEE T. Instrum. Meas.* Vol. 57, pp577-583, Mar. 2008

[2] J.k. atkinson, A.W.J. Cranny, W.V. Glasspool, and J.A. Mihell "An investigation of the performance characteristics and operational lifetimes of multi-element thick film sensor arrays used in the determination of water quality parameters", *Sensors and Actuators B: Chemical* Vol. 54, pp215-231, Mar. 1999

[3] L. Chen, and M. Mehregany, "A silicon carbide capacitive pressure sensor for in-cylinder pressure measurement" *Sensors and Actuators A:Physical,* Vol. 145, pp2-8,Aug. 2008

[4] J-F. Lei, H.A. Will "Thin-film thermocouples and strain-gauge technologies for engine applications" *Sensors and Actuators A:Physical,* Vol. 65, pp187-193 Mar. 1998

[5] J. Hodgkinson, and R.P. Tatam, "Optical gas sensing: a review", *Meas. Sci. Technol.* Vol. 24, pp012004-1-012004-59 ,Nov. 2013

[6] H. Tai, H. Tanaka, and T. yoshino, "Fiber-optic evanescent-wave methane-gas sensor using optical absorption for the 3.392-μm line of a He-Ne laser", *Opt. Lett.* Vol. 12, pp437-439, Jun. 1987

[7] M. J. Tierney, and H.O.L. Kim "Electrochemical gas sensor with extremely fast response times", *Anal. Chem.* Vol. 65, pp3435-3440, Dec. 1993

[8] K. Okamura, T. Ishiji, M. Iwaki, y. Suzuki, K. takahashi, "Electrochemical gas sensor using a novel gas permeable electrode modified by ion implantation", *Surf. Coat. Tech.* Vol. 201, pp8116-8119, Aug. 2007

[9] E. Comini, G. Faglia, and G. Sberveglieri, "Stable and highly sensitive gas

sensors based on semiconducting oxide nanobelts", *Appl. Phys. Lett.* Vol. 81, pp1869-1871, Aug. 2002

[10] J. Watson," The tin oxide gas sensor and its applications" *Sensors and Actuators*, Vol. 5, pp29-42, May 1984

[11] S.R. Aliwell, J.F. Halsall, K.F.E. Pratt, J.O' Sullican, R.L. Jones, R.A. Cox, S.R. Utembe, G.M. Hansford, and D.E. Williams, "Ozone sensors based on WO_3: a model for sensor drift and a measurement correction method", *Meas. Sci. Technol.* Vol. 12, pp684-690, Mar. 2001

[12] H. Li, Z. Yin, Q. He, H. Li, X. Huang, G. Lu, D.W.H. Fam, A. Y. Tok, Q. Zhang, and H. Zhang, "Fabrication of single- and multilayer MoS_2 film-based field-effect transistors for sensing NO at room temperature" *Small*, Vol. **8**, pp63-67, Oct. 2012

[13] X. Chen, C.K.Y. Wong, C.A. yuan, and G. Zhang, "Nanowire-based gas sensors", *Sensors and Actuators B: Chemical*, Vol. 177, pp178-195, Feb. 2013

[14] S. Maeng, "Single-walled carbon nanotube network gas sensor", *Carbon Nanotubes - Growth and Applications*, pp437-456, Aug. 2011

[15] J.-H. Lee, "Gas sensors using hierarchical and hollow oxide nanostructures: overview", *Sensors and Actuators B: Chemical*, Vol. 140, pp319-336, Jun. 2009

[16] S.C. Hernandez, D. Chaudhuri, W. Chen, N.V. Myung, and A. Mulchandani, "Single polypyrrole nanowire ammonia gas sensor", *Electroanalysis*, Vol. 19, pp2125-2130, Jul. 2007

[17] H.Y. Jeong, D.-S. Lee, H.K. Choi, D.H. Lee, J.-E. Kim, J.Y. Lee, W. J. Lee, S.O. Kim, and S.-Y. Choi "Flexible room-temperature NO_2 gas sensors based on carbon nanotubes/reduced graphene hybrid films", *Appl. Phys. Lett.* Vol. 96, pp213105-1-213105-4, May 2002

[18] S. Capone, A. Forleo, L. Francioso, P. Siciliano, J. Spadavecchia, D.S. Presicce, A. M. Taurino "Solid state gas sensors: state of the art and future activities", *J. Optoelectron. Adv. M.*, Vol. 5, pp1335-1348, Aug. 2003

[19] J. Du, Dong. Liang, H. Tang, and X. P.A. Gao, "InAs nanowire transistors as gas sensor and the response mechanism", *Nano Lett.* Vol. **9**, pp4348-4351, Sep. 2009

[20] K. I. Lundstrom, M. S. Shivaraman and C. M. Svensson, "A hydrogen-sensitive Pd-gate MOS transistor", *J. Appl. Phys.* Vol. 46, pp 3876-3881, Sep. 1975

[21] K. Tsukada, T. Kiwa, T. Yamaguchi, S. Migitaka, Y. Goto, and K. Yokosawa, "A study of fast response characteristics for hydrogen sensing with platinum FET sensor", *Sensors and Actuators B: Chemical,* Vol. 114, pp158-163, Mar. 2006

[22] Hasegawa, M. (C/O Fujitsu Limited) Semiconductor devices with silicon-on-insulator structures. *European Patent* No. 0331811 A2 ,Sep. 1989

[23] I. Eisele, and M. Zimmer, "Hybrid-gate suspended field-effect transistors for gas-sensing", *Proceedings of the 60th IEEE Device Research Conference (DRC),* pp113-116, Jun. 2002

[24] M. Burgmair, H.-P. Frerichs, M. Zimmer, M. Lehmann, and I. Eisele, "Field effect transducers for work function gas measurements: device improvements and comparison of performance" *Sensors and Actuators B: Chemical,* Vol. 95, pp183-188, Oct. 2003

[25] R. pohle, E. Simon, R. Schneider, M. Fleischer, H. Meixner, H.-P. Frerichs, and M. Lehmann, "Realization of a new sensor concept: improved CCFET and SGFET type gas sensors in hybrid flip-chip technology", *Proceedings of the 12th IEEE International Conference on Solid State Sensors, Actuators and*

Microsystems, pp135-138, Jun. 2003

[26] M. Burgmair, M. Zimmer, and I. Eisele, "Humidity and temperature compensation in work function gas sensor FETs", *Sensors and Actuators B: Chemical*, Vol. 93, pp271-275, Aug. 2003

[27] C.-H. Kim, I.-T. Cho, J. Shin, K.-B. Choi, J.-K. Lee, and J.-H. Lee, "A new gas sensor based on MOSFET having a horizontal floating-gate," *IEEE Electron Device Letters*, Vol. 35, No. 2, pp. 265-267, Feb. 2014

[28] Y. Hong, C.-H. Kim, J. Shin, K. Y. Kim, J. S. Kim, C. S. Hwang, and J.-H. Lee, "Highly selective ZnO gas sensor based on MOSFET having a horizontal floating-gate," *Sensors and Actuators B: Chemical*, Vol. 232, pp. 653-659, Apr. 2016

[29] W. Yuan, and G. Shi, "Graphene-based gas sensors", *J. Mater. Chem. A*, Vol.1, pp 10078-10091, Jun. 2013.

[30] G. Lu, L.E. Ocola, and J. Chen, "Reduced graphene oxide for room-temperature gas sensors", *Nanotechnology*, Vol. 20, pp445502-1-445502-9, Sep. 2009

[31] B. Cho, M.G. Hahm, M. Choi, J. Yoon, A.R. Kim, Y.J. Lee, S.G. Park, J.D. Kwon, C.S. Kim, M. Song, Y. Jeong, K.S. Nam, S. Lee, T.J. Yoo, C.G. Kang, B.Y. Lee, H.C. Ko, P.M. Ajayan, and D.H. Kim, "Charge-transfer-based Gas Sensing Using Atomic-layer MoS_2", *Sci. Rep.*, Vol. 5, pp8052-1-8052-6, Jan. 2015

[32] Y. Hong, W.-M. Kang, I.-T. Cho, J. Shin, M. Wu, and J.-H. Lee, “Gas-Sensing characteristics of Exfoliated WSe_2 Field Effect Transistors”, *Journal of Nanoscience and Nanotechnology*, Vol. 17, pp. 3151-3154, May 2017

[33] H. yamaura, T. Jinkawa, J. Tamaki, k. Moriya, N. Miura, and N. yamazoe, "Indium oxide-based gas sensor for selective detection of CO", *Sensors and Actuators B: Chemical*, Vol.36, pp 325-332, Oct. 1996

[34] J. Kukkola, J. Maklin, N. Halonen, T. Kyllonen, G. Toth, M. Szabo, A. Shchukarev, J.-P. Mikkola, H. Jantunen, and K. Kordas "Gas sensors based on anodic tungsten oxide", *Sensors and Actuators B: Chemical*, Vol.153, pp 293-300, Apr. 2011

[35] R. Kumar, O.A. Dossary, G. Kumar, and A. Umar "Zinc Oxide nanostructures for NO_2 gas sensor applications: A review", *Nano-Micro Lett.*, Vol. 7, pp97-120, Apr. 2015

[36] J.S. Suehle, R.E. Cavicchi, M. Gaitan, and S. Semancik, "Tin oxide gas sensor fabricated using CMOS micro-hotplates and *in-situ* processing", *IEEE Electron Device Letters*, Vol.14, pp 118-120, Mar. 1993

[37] T. Maruyama, S. Sasaki, and Y. Saito, "Potentiometric gas sensor for carbon dioxide using solid electrolytes", *Solid State Ionics*, Vol. 23, pp107-112, Mar. 1987

[38] J.-H. Lee " Gas sensors using hierarchical and hollow oxide nanostructures : Overview", *Sensors and Actuators B: Chemical*, Vol.140, pp 319-336, Jun. 2009

[39] A. Star, V. Joshi, S. Skarupo, D. Thomas, and J.-C.P. Gabriel, "Gas sensor array based on metal-decorated carbon nanotubes", *J. Phys. Chem. B*, Vol. 110, pp21014-21020, Aug. 2006

[40] S. Park, S. Kim, W.I. Lee, K.-K Kim, and C. Lee, "Room temperature, ppb-level NO_2 gas sensing of multiple-networked ZnSe nanowire sensors under UV illumination", *J. Nanotechnol.*, Vol. 5, pp1836-1841, Oct. 2014

[41] S. Zhang, C. Xie, G. Zhang, Q. Zhu, and S. Zhang, "Assessing multi-variable coupling effects of UV illumination, heat and oxygen on porous ZnO

nanocrystalline film through electron concentration and mobility extraction", *Phys. Chem.Chem. Phys.*, Vol. 17, pp18045-08054, Jun. 2015

[42] W.-J. Hwang, K.-S. shin, J.-H. Roh, D.-S. Lee, and S.-H. Choa, "Development of Micro-heaters with optimized temperature compensation design for gas sensors", *Sensors*, Vol.11, pp2580-2591, Mar. 2011

[43] S. Santra, A.D. Luca, S. Bhaumik, S.Z. Ali, F. Udrea, J.W. Gardner, S.K. Ray, and P.K. Guha, "Dip pen nanolithography-deposited zince oxide nanorods on a CMOS MEMS platform for ethanol sensing", *RSC Adv.*, Vol. 5, pp47609-47616, May 2015

[44] M. Itsumi and F. Kiyosumi, "Identification and elimination of gate oxide defect origin produced during selective field oxidation," *J. Electrochem.Soc.*, Vol. 129, pp. 800–806, Apr. 1982

[45] J.-H. Lee, S.-Y. Kim, I.-H. Cho, S.-B. Hwang, and J.-H. Lee, "l/f noise characteristics of sub-100 nm MOS transistors", *J. Semicond. Techno. Sci*., Vol. 6, pp38-42, 2006

[46] B. Cretu, M. Fadlallah, G. Ghibaudo, J. Jomaah, F. Balestra, and G. Guegan, "Thorough characterization of deep-submicron surface and buried channel pMOSFETs", *Solid State Electronics*, Vol. 46, pp971-975, Jul. 2002

[47] C. Wang, L. Yin, L. Zhang, D. Xiang, and R. Gao, "Metal oxide gas sensor : Sensitivity and Influencing factors", *Sensors*, Vol. 10, pp2088-2106, Mar. 2010

[48] N. Barsan, D. Koziej, U. Weimar, "Metal oxide-based gas sensor research: How to?", *Sensors and Actuators B: Chemical*, Vol. 121, pp. 18-35, Oct. 2006

[49] H.-J. Kim, H.-M. Jeong, T.-H. Kim, J.-H. Chung, Y.C. Kang, and J.-H. Lee, "Enhanced ethanol sensing characteristics of In_2O_3-decorated NiO hollow nanostructures via modulation of hole accumulation layer", *ACS Appl. Mater. & Interfaces*, Vol. 6, pp. 18197-18204, Sep. 2014

[50] W. Yuan, and G. Shi, "Graphene-based gas sensors", *J. Mater. Chem. A*, Vol. 1, pp. 10078-10097, Jun. 2013

[51] Y. Sun, and H.H. Wang, "Electrodeposition of Pd nanoparticles on sigle-walled carbon nanotubes for flexible hydrogen sensors", *Applied Physics Letters*, Vol. 1, pp. 10078-10097, Jun. 2013

[52] Y.R. Choi, Y. -G. Yoon, K. S. Choi, J. H. Kang, Y. -S. Shim, Y. H. Kim, H. J.Chang, J. -H. Lee, C. R. Park, S. Y. Kim, and H. W. Jang, "Role of ooxygen functional group in graphene oxide for reversible room-temperature NO_2 sensing", *Carbon*, Vol. 91, pp. 178-187, May, 2015

[53] Z. Tang, L.Y. Sheng, C. H. Philip, C.H. Chan, and K.O.S. Johnny, "A CMOS compatible integrated gas sensor", *Proceedings 1996 IEEE Hong Kong Electron Devices Meeting*, pp9-12, Jun. 1996

[54] J. Shin, Y. Hong, M. Wu, Y. Jang, J.S. Kim, B.-G. Park, C. S. Hwang, and J.-H. Lee, "Highly Improved Response and Recovery Characteristics of Si FET-type Gas Sensor Using Pre-bias," *2016 International Electron Devices Meeting*, pp. 18.1.1-18.1.4, Dec. 2016

[55] M. Wu, C.-H. Kim, J. Shin, Y. Hong, X. Jin, J.-H. Lee, "Effect of a pre-bias on the adsorption and desorption of oxidizing gases in FET-type sensor," *Sensors and Actuators B: Chemical*, Vol. 245, pp. 122-128, Jan. 2017

[56] M. Wu, J. Shin, Y. Hong, X. Jin, and J.-H. Lee, "Pulse Biasing Scheme for the Fast Recovery of FET-Type Gas Sensors for Reducing Gases," *IEEE Electron Device Letters*, Vol. 38, pp. 971-974, Jul. 2017

[57] Y. Hong, C.-H. Kim, S.-J. Choi, I.-D. Kim and Jong-Ho Lee, "Tin dioxide gas sensor prepared by inkjet printing method," *2014 the 7th Asia-Pacific conference on Transducers and Micro/Nano Technologies (APCOT)*, Jun. 2014

[58] J. Shin, Y. Hong, M. Wu, and J.-H. Lee, "A Wide Detection Range Mercury Ion Sensor Using Si MOSFET Having Single-Walled Carbon Nanotubes as a Sensing Layer," *IEEE Electron Device Letters*, Vol. 38, No. 7, pp. 959-962, Jul. 2017

[59] Neudeck, P. G. et al. "High-temperature electronics—a role for wide bandgap semiconductors", *P. IEEE*, Vol. 90, pp1065-1076 (2002)

[60] N.M. Shaalan, T. Yamazaki, and T. Kikuta, "Influence of morphology and structuregeometry on NO_2 gas-sensing characteristics of SnO_2 nanostructures synthesized via a thermal evaporation method, *Sensors and Actuators B: Chemical*, Vol. 153, pp11–16, Mar. 2011

[61] F.B. Oruc, L.E. Aygun, I. Donmez, N. biyikli, A.K. Okyay, and H.Y. Yu, "Low temperature atomic layer deposited ZnO photo thin film transistors," *J. Vac. Sci. Technol. A*, Vol. 33, pp01A105-1-01A105-5, Aug. 2014

List of Publications

Journals

1. **Jongmin Shin**, Yoonki Hong, Meile Wu, Jong-Ho Bae, Hyuck-In Kwon, Byung-Gook Park, and Jong-Ho Lee, “An accurate and stable humidity sensing characteristics of Si FET-type humidity sensor with MoS_2 as a sensing layer by pulse measurement”, *Sensors and Actuators B: Chemical*, Vol. 258, pp. 574-579, Apr. 2018

2. Meile Wu, **Jongmin Shin**, Yoonki Hong, Dongkyu Jang, Xiaoshi Jin, Hyuck-In Kwon ,and Jong-Ho Lee, “An FET-Type Gas Sensor with a Sodium Ion Conducting Solid Electrolyte for CO_2 Detection”, *Sensors and Actuators B: Chemical*, Vol. 259, pp. 1058-1065, Apr. 2018

3. **Jongmin Shin**, Yoonki Hong, Meile Wu, and Jong-Ho Lee, "A Wide Detection Range Mercury Ion Sensor Using Si MOSFET Having Single-Walled Carbon Nanotubes as a Sensing Layer," *IEEE Electron Device Letters*, Vol. 38, No. 7, pp. 959-962, Jul. 2017

4. Meile Wu, **Jongmin Shin**, Yoonki Hong, Xiaoshi Jin, and Jong-Ho Lee, "Pulse Biasing Scheme for the Fast Recovery of FET-Type Gas Sensors for Reducing Gases," *IEEE Electron Device Letters*, Vol. 38, pp. 971-974, Jul. 2017

5. Meile Wu, Chang-Hee Kim, **Jongmin Shin**, Yoonki Hong, Xiaoshi Jin, Jong-Ho Lee, "Effect of a pre-bias on the adsorption and desorption of oxidizing gases in FET-type sensor," *Sensors and Actuators B: Chemical*, Vol. 245, pp. 122-128, Jan. 2017

6. Yoonki Hong, Won-Mook Kang, In-Tak Cho, **Jongmin Shin**, Meile Wu, and Jong-Ho Lee, “Gas-Sensing characteristics of Exfoliated WSe2 Field Effect Transistors”, *Journal of Nanoscience and Nanotechnology*, Vol. 17, No. 5,

pp. 3151-3154, May 2017

7. Kyu-Bong Choi, **Jongmin Shin**, and Jong-Ho Lee, "Analysis of Current Fluctuation Due to Trap and Percolation Path in Nano-Scale Bulk FinFET," *Journal of Nanoscience and Nanotechnology*, Vol. 16, No. 5, pp. 4803-4807, May 2016

8. Yoonki Hong, Chang-Hee Kim, **Jongmin Shin**, Kyoung Yeon Kim, Jun Shik Kim, Cheol Seong Hwang, and Jong-Ho Lee, "Highly selective ZnO gas sensor based on MOSFET having a horizontal floating-gate," *Sensors and Actuators B: Chemical*, Vol. 232, pp. 653-659, Apr. 2016

9. Sung Hun Jin, Seung-Kyun Kang, In-Tak cho, Sang Youn Han, Ha Uk Chung, Dong Joon Lee, **Jongmin Shin**, Geun Woo Baek, Tae-il kim, Jong-Ho Lee, and John A. Rogers, "Water-soluble thin film transistors and circuits based on amorphous Indium-Galium-Zinc Oxide, *ACS Appl. Mater. Interfaces*, Vol. 7, No. 15, pp 8268-8274, March, 2015

10. Sung Hun Jin*, **Jongmin Shin***, In-Tak Cho, Sang Youn Han, Dong Joon Lee, Chi Hwan Lee, Jong-Ho Lee, and John A. Rogers, "Solution-processed single-walled carbon nanotube field effect transistors and bootstrapped inverters for disintegratable, transient electronics," *Applied Physics Letters*, Vol. 105, No. 1, pp. 013506-1-013506-4, Jul. 2014 ***Sung Hun Jin and Jongmin Shin contributed equally to this work.**

11. Chang-Hee Kim, In-Tak Cho, **Jongmin Shin**, Kyu-Bong Choi, Jung-Kyu Lee, and Jong-Ho Lee, "A new gas sensor based on MOSFET having a horizontal floating-gate," *IEEE Electron Device Letters*, Vol. 35, No. 2, pp. 265-267, Feb. 2014

Conferences

1. Meile Wu, **Jongmin Shin**, Yoonki Hong, Dongkyu Jang, Seongbin Hong, Yujeong Jeong ,and Jong-Ho Lee, “An FET-type sensor with Pt doped In_2O_3 nanoparticles for room temperature hydrogen sensing”, *2017 The Korean Sensors Society*, Nov. 2017

2. Yujeong Jeong, **Jongmin Shin**, Yoonki Hong, Meile Wu, Seongbin Hong, and Jong-Ho Lee, “Common Source Amplifier Circuit Integrated with the Gas Sensor”, *2017 The Korean Sensors Society*, Nov. 2017

3. Seongbin Hong, **Jongmin Shin**, Yoonki Hong, Meile Wu, Dongkyu Jang, Yujeong Jeong, Hyuck-In Kwon, and Jong-Ho Lee, “Si-FET-type gas sensor with a horizontal floating gate structure for detecting carbon monoxide”, *2017 The Korean Sensors Society*, Nov. 2017

4. **Jongmin Shin**, Yoonki Hong, Meile Wu, Byung-Gook Park, and Jong-Ho Lee, "Response characteristics of Si FET-type humidity sensor having sputtered MoS_2 film as a sensing layer," *Korean Conference on Semiconductors*, Feb. 2017

5. Young-tak Seo, Yoonki Hong, **Jongmin Shin**, Dongkyu Jang, Yujeong Jeong, Seongbin Oh and Jong-Ho Lee, "Sensing characteristics of MOSFET gas sensor having inkjet-printed CNT as a sensing layer," *Korean Conference on Semiconductors*, Feb. 2017

6. **Jongmin Shin**, Yoonki Hong, Meile Wu, Younjin Jang, Jun Shik Kim, Byung-Gook Park, Cheol Seong Hwang, and Jong-Ho Lee, "Highly Improved Response and Recovery Characteristics of Si FET-type Gas Sensor Using Pre-bias," *2016 International Electron Devices Meeting*, pp. 18.1.1-18.1.4, Dec. 2016

7. **Jongmin Shin**, Yoonki Hong, Meile Wu and Jong-Ho Lee, "Sensing characteristic of lead ion using Si *p*MOSFET sensor under the different control-gate biases", *The 16th International Meeting on Chemical Sensors*,

Jul. 2016

8. Yoonki Hong, **Jongmin Shin**, Meile Wu, Soo Ho Choi, Yunsik Choi, Seungil Moon, Woochul Yang and Jong-Ho Lee, "MOSFET-based humidity sensor with inkjet-printed polymer as a sensing layer," *The 16th International Meeting on Chemical Sensors*, Jul. 2016

9. Jong-Ho Lee, Yoonki Hong, Meile Wu and **Jongmin Shin**, "High Perfomance Gas Sensors Based on Si MOSFETs," *The 16th International Meeting on Chemical Sensors*, Jul. 2016

10. Meile Wu, **Jongmin Shin**, Yoonki Hong, Xiaoshi Jin and Jong-Ho Lee, "Effect of APTES Layer on I-V Characteristics of MOSFET-type Gas Sensor Having Solid Electrolyte Sensing Material," *NANO Korea*, Jul. 2016

11. **Jongmin Shin**, So-Ong Kim, Yoonki Hong, Tai Hyun Park, and Jong-Ho Lee, "Bio-electronic nose based on Si MOSFET having a horizontal floating gate," *Korean Conference on Semiconductors*, Feb. 2016

12. Chang-Hee Kim, Yoonki Hong, **Jongmin Shin**, In-Tak Cho, Un Ki Kim, Cheol Seong Hwang, and Jong-Ho Lee, "A MOSFET type gas sensor having a horizontal floating based on ZnO," *Korean Conference on Semiconductors*, Feb. 2015

13. Kyu-Bong Choi, **Jongmin Shin**, and Jong-Ho Lee, "Analysis of current fluctuation due to trap and percolation path in nano-scale bulk FinFET," *Korean Conference on Semiconductors*, Feb. 2015

14. Chang-Hee Kim, Chul-Heung Kim, Yoonki Hong, **Jongmin Shin**, Kyu-Bong Choi, In-Tak Cho, Chul-Ho Won, Do-Kywn Kim, Jung-Hee Lee, and Jong-Ho Lee, "AlGaN/GaN MISFET gas sensor having a horizontal floating gate," *International Conference on Electronics, Information and Communication(ICEIC)*, Jan. 2015

15. Chang-Hee Kim, In-Tak Cho, **Jongmin Shin**, Kyu-Bong Choi, and Jong-Ho Lee, "A study of gas sensing property of gas FET having horizontal floating

gate," *NANO Korea*, Jul. 2014

16. **Jongmin Shin** and Jong-Ho Lee, "Impedance characteristics of GSG electrodes for RLGC modeling of cell-electrode interface," *Korean Conference on Semiconductors*, Feb. 2014

17. Jong-Ho Bae, Sunkyu Hwang, **Jongmin Shin**, Hyuck-In Kwon, Chan Hyeong Park, Hyoji Choi, Jong-Bong Park, Jongseob Kim, Jongbong Ha, Kiyeol Park, Jaejoon Oh, Jaikwang Shin, U-In Chung, Kwang Seok Seo, and Jong-Ho Lee, "Analysis of DC/Transient current and RTN behaviors related to traps in p-GaN Gate HEMT," *IEEE International Electron Devices Meeting*, pp. 31.6.1-31.6.4, Dec. 2013

18. Jong-Ho Lee, Kyu-Bong Choi, and **Jongmin Shin**, "Design and analysis of nano-scale bulk FinFETs," *International Conference on ASIC*, pp. 492-494, Oct. 2013

19. Jong-Ho Bae, Injun Hwang, **Jongmin Shin**, Hyuck-In Kwon, Chan Hyeong Park, Jongbong Ha, JaeWon Lee, Hyoji Choi, Jongseob Kim, Jong-Bong Park, Jaejoon Oh, Jaikwang Shin, U-in Chung, and Jong-Ho Lee, "Characterization of traps and trap-related effects in recessed-gate normally-off AlGaN/GaN-based MOSHEMT," *IEEE International Electron Devices Meeting*, pp. 13.2.1-13.2.4, Dec. 2012

20. Jong-Ho Lee, Kyu-Bong Choi, and **Jongmin Shin**, "Design of 14 nm tri-gate transistors on bulk wafer (Bulk FinFETs)," *NANO Korea*, Aug. 2012

Patents

1. Jong-Ho Lee, and **Jongmin Shin**, “Pulse Method for FET-type Sensor Having Horizontal Floating Gate”
   - (US) 15 612.384
   - (KR) Patent Publication No. 10-2017-0068246

초 록

최근 자동차 배기가스, 대기오염, 농업, 가전 제품 등에 가스센서 기술이 점점 중요해지고 있다. 따라서 많은 연구 그룹에서 광, 전기화학, 반도체 및 FET기반의 가스센서와 같은 형태의 가스센서 연구가 보고되고 있다. 그러나 대부분의 연구는 센서의 구조나 감지 물질에 대한 연구가 주를 이루고 있다. 현재 가장 많이 연구되고 있고, 양산 중인 저항형 가스센서는 크기, 수율, 및 신호 처리회로와의 호환성이 낮다는 단점이 있기 때문에 저가격, 고 신뢰성, CMOS센서 처리회로와의 호환성이 높은 실리콘 FET형 가스센서에 대한 관심이 증가 하고 있다. 하지만 FET형 가스센서는 4개의 단자로부터 오는 높은 전기적 자유도를 가지지만, 센서의 성능을 향상시키기 위한 보고는 없었다.

따라서, 본 논문에서는 수평형 플로팅 게이트를 가지는 실리콘 FET형 가스센서의 가스 반응 및 회복 특성을 향상 시키기 위한 펄스 프리바이어스 (V_{pre}) 방법을 최초로 제안하고 가스 응답 특성 및 복구 특성을 측정 및 분석 하였다. 프리바이어스의 효과를 알아보기 위해 제작된 실리콘 FET형 가스센서는 수평방향으로 제어 전극과 플로팅 전극을 가지고 있고, 감지 물질로 사용된 ZnO막은 ALD방법을 통해 제어 전극과 플로팅 전극 사이에 형성 되었다. 제어 전극에 펄스 프리바이어스 방법을 인가하여 그 효과를 검증 하였고, ZnO와 산화성 가스인 NO_2가스의 반응을 분석하였다. 프리바이어스 효과에 대한 반응 메커니즘은 에너지 밴드 다이어그램을 통하여 설명하였다. 산화성 가스에

대한 반응성을 높이기 위해 제어전극에 음의 프리바이어스를 인가하여 주고, 회복 시간을 줄이기 위해서 양의 프리바이어스를 인가하여 줌으로써 FET형 가스센서의 센싱 성능을 향상 시킬 수 있었다. 또한, 음의 프리바이어스를 인가하여 반응 시킬 경우 아주 낮은 농도의 NO_2농도의 검출이 가능하였고, 양의 프리바이어스를 인가하여 회복 시킨 경우 온도를 높여서 가스를 회복 시킨 것과 같은 효과를 보여주었다. 이외에도 프리바이어스에 영향을 줄 수 있는 여러가지 요인들에 대한 측정을 통해 프리바이어스 효과가 산화성 가스의 반응 및 회복에 큰 영향을 주는 것을 검증 하였다. 본 실험에서 사용한 감지 물질 이외에도 다양한 감지 물질을 증착하여 측정한 결과 프리바이어스가 매우 효과적임을 알 수 있었다.

제안된 방법은 표적가스의 NO_2에 대한 가스 반응을 향상 시키고, 회복 시간을 크게 감소 시키는데 매우 효과적임을 입증 하였다. 프리바이어스 방법은 FET형 가스센서의 상용화에 시키는데 매우 효과적일 것으로 기대된다.

주요어 : 프리바이어스 펄스 방법, FET형 가스센서, 전자 축적, 전자 공핍, 일함수 변화, 용량 변화

학번 : 2012-20801